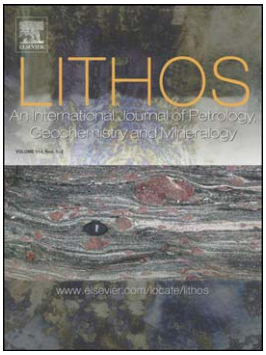

Eocene magmatic processes and crustal thickening in southern Tibet: Insights from strongly fractionated ca. 43 Ma granites in the western Gangdese Batholith

Qing Wang, Di-Cheng Zhu, Peter A. Cawood, Zhi-Dan Zhao, Sheng-Ao Liu, Sun-Lin Chung, Liang-Liang Zhang, Dong Liu, Yuan-Chuan Zheng, Jin-Gen Dai

PII: S0024-4937(15)00364-3
DOI: doi: 10.1016/j.lithos.2015.10.003
Reference: LITHOS 3714

To appear in: *LITHOS*

Received date: 27 July 2015
Accepted date: 15 October 2015

Please cite this article as: Wang, Qing, Zhu, Di-Cheng, Cawood, Peter A., Zhao, Zhi-Dan, Liu, Sheng-Ao, Chung, Sun-Lin, Zhang, Liang-Liang, Liu, Dong, Zheng, Yuan-Chuan, Dai, Jin-Gen, Eocene magmatic processes and crustal thickening in southern Tibet: Insights from strongly fractionated ca. 43 Ma granites in the western Gangdese Batholith, *LITHOS* (2015), doi: 10.1016/j.lithos.2015.10.003

Eocene magmatic processes and crustal thickening in southern Tibet: Insights from strongly fractionated ca. 43 Ma granites in the western Gangdese Batholith

Qing Wang[a,*], Di-Cheng Zhu[a,*], Peter A. Cawood[b], Zhi-Dan Zhao[a], Sheng-Ao Liu[a], Sun-Lin Chung[c], Liang-Liang Zhang[a], Dong Liu[a], Yuan-Chuan Zheng[a], Jin-Gen Dai[a]

[a] State Key Laboratory of Geological Processes and Mineral Resources, and School of Earth Science and Resources, China University of Geosciences, Beijing 100083, China

[b] Department of Earth Sciences, University of St Andrews, North Street, St Andrews KY16 9AL, UK

[c] Department of Geosciences, National Taiwan University, Taipei 106, China

Revised manuscript submitted to Lithos (October 14, 2015)

*Corresponding authors: **Qing Wang and Di-Cheng Zhu**

State Key Laboratory of Geological Processes and Mineral Resources
China University of Geosciences
29# Xue-Yuan Road, Haidian District
Beijing 100083, China
Phone: (+86-10) 8232 2094 (O)
Fax: (+86-10) 8232 2094
Email: qing726@126.com, dchengzhu@163.com

ABSTRACT

This study reports zircon U-Pb age and Hf isotope, whole-rock major and trace element, and Sr-Nd-Pb-Hf isotope data for the Dajia pluton, western Gangdese Batholith, in southern Tibet. These data indicate that the pluton consists of moderately (Group 1) and strongly (Group 2) fractionated granites that were emplaced synchronously at ca. 43 Ma. The Group 1 samples have SiO_2 contents of 69–72 wt.% and vary in terms of the differentiation index (DI = 84–93). These rocks are depleted in Ba, Nb, Sr, P, and Ti, with moderate negative Eu anomalies, and display low heavy rare earth elements (HREEs) and Y abundances. The Group 2 samples are characterized by high SiO_2 (75–78 wt.%) and DI (95–97); significantly negative Eu anomalies; marked concave-upward middle REE (Gd-Ho) patterns; and Ba, Sr, P, and Ti anomalies that are significantly more negative than those of the Group 1 samples. The Group 1 samples have whole-rock $\varepsilon_{Nd}(t)$ (-5.9 to -6.0), $\varepsilon_{Hf}(t)$ (-4.0 to -4.5), and zircon $\varepsilon_{Hf}(t)$ (-6.0 to +5.8) values identical to those of the Group 2 samples [$\varepsilon_{Nd}(t)$ = -5.7 to -6.7, $\varepsilon_{Hf}(t)$ = -3.5 to -2.9, and zircon $\varepsilon_{Hf}(t)$ = -2.0 to +4.2], as well as similar initial Pb isotopic compositions. These data indicate that the two groups were derived from a common source region with garnet as a residual mineral phase. The Group 1 samples were most likely derived from partial melting of garnet-bearing amphibolite (rather than eclogite) within the juvenile southern Lhasa crust and mixed with the enriched components from the subducting ancient Indian continental crust and/or the ancient central Lhasa basement. The Group 2 samples are interpreted as the products of extensive fractional crystallization (plagioclase, K-feldspar, biotite, apatite, allanite, titanite, monazite, and ilmenite) of the melts represented by the Group 1 samples. Low HREEs and Y abundances of the Dajia pluton, together with the presence of strongly fractionated granites (Group 2) identified for the first time in the Gangdese Batholith, indicate that the crust beneath the Dajia region had already been thickened by ca. 43 Ma. High whole-rock zircon saturation temperatures (815°C–869°C) of the Group 1 samples and the other ca. 43 Ma coeval magmatism documented both in the Gangdese Batholith and in the Tethyan Himalaya can be best interpreted as the final consequences of the magmatic responses to the Neo-Tethyan oceanic slab breakoff.

Keywords: Mid-Eocene; Strongly fractionated granites; Crustal thickening; Gangdese Batholith; Southern Tibet

1. Introduction

The Tibetan Plateau is the world's highest and largest plateau. It has the thickest continental crust on Earth at 60−80 km, which is twice the normal crustal thickness. However, the timing of crustal thickening of the plateau with respect to the India-Asia collision is under debate. For example, structural geological studies suggested that the thickening of the crust in the Lhasa terrane of the plateau might have initiated prior to the mid-Cretaceous (ca. 100 Ma), before the India-Asia collision (Murphy et al., 1997; Kapp et al., 2005). In contrast, petrological and geochemical studies of the central and eastern Gangdese Batholith in southern Tibet have proposed varying ages for crustal thickening, ranging from 62 Ma to 25 Ma (Mo et al., 2007; Chung et al., 2009; Guan et al., 2012; Ji et al., 2012; Jiang et al., 2014), which cover the time frame from pre- to post-collision (cf. Zhu et al., 2015 and references therein).

The voluminous Gangdese Batholith documents both the Neo-Tethyan oceanic subduction and collisional history of India-Asia interaction and provides a direct temporal and spatial magmatic record of the crustal evolution in southern Tibet (Yin and Harrison, 2000; Chung et al., 2005; Ji et al., 2009; Zhu et al., 2011, 2013, 2015). However, to date, studies of the batholith have focused on the central and eastern portions (Chung et al., 2009; Guan et al., 2012; Ji et al., 2012; Jiang et al., 2014), and little or no information about the western portion is available. It has been recognized that the Gangdese Batholith is continuous in composition from gabbro to granite, and is dominated by biotite–hornblende-bearing diorite and granodiorite (Chung et al., 2003; Mo et al., 2005; Chu et al., 2006; Ji et al., 2009, 2012; Wen, 2007; Wen et al., 2008a; Zhu et al., 2011, 2013; Jiang et al., 2014). Such a rock association, together with the identical isotopic compositions from gabbro to granite (Mo et al., 2009; Niu et al., 2013), inhibits detailed investigations of the magmatic processes operating during the emplacement of the Gangdese Batholith through isotopic data.

In this paper, we present zircon U-Pb age and Hf isotope, whole-rock major and trace element, and Sr-Nd-Pb-Hf isotope data for the Dajia pluton in the western Gangdese Batholith. Our dataset reveals for the first time the presence of ca. 43 Ma strongly fractionated granites and moderately fractionated granites with low HREEs and Y abundances, placing vital constraints on the magmatic processes and petrogenesis of the Gangdese Batholith and on the crustal thickening of the southern Lhasa Terrane by ca. 43 Ma.

2. Geological background and samples

The Tibetan Plateau is a tectonic collage of five W-E trending tectonic belts, which from north to south include the Songpan–Ganzi flysch complex, the Eastern Qiangtang, the Western Qiangtang, the Lhasa Terrane, and the Himalaya (cf. Zhu et al., 2013). These five blocks or terranes are separated by the Jinsha (JSSZ), Longmu Tso−Shuanghu (LSSZ), Bangong–Nujiang (BNSZ), and Indus–Yarlung Zangbo (IYZSZ) suture zones, all of which represent the remnants of the Tethyan ocean basin (Fig. 1a) (cf. Yin and Harrison, 2000; Deng et al., 2014; Zhu et al., 2013).

According to the differences of basement rock and sedimentary cover, the Lhasa Terrane can be further divided into northern, central, and southern subterranes, separated by the Shiquan River–Nam Tso Mélange Zone (SNMZ) and Luobadui–Milashan Fault (LMF), respectively (Fig. 1b) (Zhu et al., 2009, 2011, 2013). The northern Lhasa subterrane contains Middle Triassic–Cretaceous sedimentary rocks with abundant Early Cretaceous volcanic rocks and associated coeval granitoids built on a juvenile crust (cf. Pan et al., 2004; Zhu et al., 2011, 2013; Sui et al., 2013). The central Lhasa subterrane was once a microcontinent with Archean-Proterozoic basement rocks (Zhu et al., 2009, 2011, 2013). Such basement rocks are covered mainly by Permo-Carboniferous metasedimentary and Upper Jurassic−Lower Cretaceous sedimentary units with abundant volcanic rocks (Zhu et al., 2009, 2011, 2013) plus minor Ordovician, Silurian, Devonian, and Triassic limestone (cf. Pan et al., 2004) and rare Cambrian strata (cf. Zhu et al., 2012). The southern Lhasa subterrane is also characterized by the presence of juvenile crust (cf. Ji et al., 2009; Zhu et al., 2011) with a Precambrian crystalline basement locally preserved in its eastern segment (Dong et al., 2010; Zhu et al., 2013). This subterrane is dominated by the Gangdese Batholith and the Paleogene Linzizong volcanic succession (cf. Chung et al., 2005; Mo et al., 2008; Ji et al., 2009; Lee et al., 2009; Zhu et al., 2011, 2013, 2015), along with minor Triassic–Cretaceous volcano-sedimentary rocks (cf. Pan et al., 2004; Zhu et al., 2008, 2013). Tectonically, both the northern and southern Lhasa subterranes experienced significant crustal shortening (>50% and >40%, respectively) from the Late Cretaceous to the Paleocene (ca. 90-69 Ma; cf. Kapp et al., 2003, 2007; He et al., 2007; Volkmer et al., 2007).

The Gangdese Batholith extends for more than 1500 km along the southern Lhasa

subterrane and locally intrudes into the Triassic-Cretaceous volcano-sedimentary sequence (e.g., Yeba Formation and Sangri Group). Recent zircon U-Pb geochronological data indicate that this batholith was emplaced from the Late Triassic (ca. 205 Ma) to the Miocene (ca. 13 Ma) (cf. Chung et al., 2005; Wen et al., 2008a; Ji et al., 2009; Zhu et al., 2011).

The Dajia pluton is exposed in Dajia village of the western Gangdese Batholith (Fig. 1b). These rocks are faulted against Paleocene andesites and rhyolitic pyroclastic rocks within the lower part (Dianzhong Formation) of the Linzizong volcanic succession (Fig. 1c). The Dajia pluton consists of medium- and coarse-grained monzogranites and syenogranites with porphyritic texture. These rocks are pale, flesh-colored and grayish white and contain plagioclase and K-feldspar megacrysts (Figs. 2a-b). The main minerals in the monzogranites are plagioclase (20–40%), K-feldspar (25–35%), quartz (25–40%), and minor amounts of biotite (< 5%). Accessory minerals include apatite, zircon, titanite, and Fe–Ti oxides. The syenogranites contain 40–60% K-feldspar, 20–25% plagioclase, 30–35% quartz, and trace amounts of biotite (< 1%), with accessory apatite, zircon, titanite, and iron oxides.

3. Analytical methods and results

3.1. Zircon geochronological data

Two monzogranite samples (12DJC13-2 and 12DJC14-2) and one syenogranite sample (12DJC12-1) were selected for zircon LA-ICPMS U–Pb dating (Table S1). The descriptions of the analytical methods used are given in Appendix A. Zircon grains are mostly euhedral to subhedral, with crystal lengths of 50–200 μm and length-to-width ratios from 1:1 to 2:1, and exhibit clear oscillatory zoning (Figs. 3a-c). All of the analyzed zircons have varying Th (1055–7438 ppm) and U (1635–9964 ppm) abundances, with Th/U ratios ranging from 0.24 to 1.91 (Table S1), consistent with a magmatic origin (Hoskin and Schaltegger, 2003). No old zircons with inherited cores were identified in the dated samples. Thus, the obtained ages are considered to represent the timing of zircon crystallization, which in turn represents the timing of the granite crystallization.

The analyses of 14 zircons from sample 12DJC12-1 yield $^{206}Pb/^{238}U$ ages ranging from 41.7 to 43.5 Ma, with a weighted mean age of 42.6 ± 0.3 Ma (MSWD =

1.3) (Fig. 3a). A similar age of 42.7 ± 0.4 Ma (MSWD = 0.9) was also obtained for sample 12DJC13-2, with a range of $^{206}Pb/^{238}U$ ages of 41.7 to 43.9 Ma for 12 analyses (Fig. 3b). The analyses of 18 zircons from sample 12DJC14-2 plot on or close to the concordant curve and yield $^{206}Pb/^{238}U$ ages ranging from 42 Ma to 45 Ma, with a weighted mean of 43.6 ± 0.5 Ma (MSWD = 0.5) (Fig. 3c).

One syenogranite sample (08CQ02) reported by Zhu et al. (2011) gave a weighted mean $^{206}Pb/^{238}U$ age of 43.9 ± 0.3 Ma (MSWD = 1.8), similar to the $^{206}Pb/^{238}U$ ages of the three samples reported here. Thus, both the monzogranites and the syenogranites were emplaced synchronously at ca. 43 Ma.

3.2. Whole-rock geochemical data

Analytical methods are described in Appendix A and data for whole-rock major and trace elements are given in Table S2.

Samples from the Dajia pluton can be classified into two groups on the basis of geochemical compositions. Group 1 includes four monzogranite and two syenogranite samples (Fig. 4a) and has high-K calc-alkaline affinity (Fig. 4b) with K_2O/Na_2O of 1.28–1.61. These samples have SiO_2 of 69–72 wt.% and varying A/CNK ratios (1.03–1.23) and are moderately fractionated in composition as indicated by a differentiation index (DI) of 84–93 (Fig. 4c). The Al_2O_3, CaO, TiO_2, and P_2O_5 of this group show negative correlations with SiO_2 (Figs. 5a-d). Group 1 has Y abundances of 10–19 ppm, varying light REEs enrichment ($[La/Yb]_N$ = 18.1–26.9, where N denotes normalized to chondrite values of Sun and McDonough [1989]), and moderate negative Eu anomalies (Eu/Eu* = 0.56–0.78) (Figs. 5f and 6a). The samples in this group are enriched in Rb, Th, and U and depleted in Ba, Nb, Sr, P, and Ti (Fig. 6b).

Group 2 consists of eight high-K calc-alkaline syenogranite samples (Figs. 4a-b) and is strongly fractionated in composition, as indicated by its high SiO_2 (75–78 wt.%) and DI (95–97) (Fig. 4c). Negative correlations between SiO_2 and oxides (e.g., TiO_2, Al_2O_3, CaO, and P_2O_5) are present (Figs. 5a-d). This group is characterized by low abundances of Y (6–15 ppm), strong negative Eu anomalies (Eu/Eu* = 0.26–0.66) (Fig. 6a), and significantly negative Ba, Sr, P, and Ti anomalies (Fig. 6b). The samples in this group display distinct concave-upward middle REE (Gd-Ho) patterns, which are not observed in Group 1.

3.3. Whole-rock Sr-Nd-Pb-Hf isotopic data

Analytical methods for whole-rock Sr-Nd-Pb-Hf isotopic determination are given in Appendix A, and the results are listed in Table S3. Initial isotopic ratios were calculated for the age of 43 Ma.

The measured $^{87}Sr/^{86}Sr$ ratios of the Group 1 samples are 0.71036–0.71120, with $^{87}Rb/^{86}Sr$ ratios ranging from 4.6 to 7.2, yielding initial $^{87}Sr/^{86}Sr$ ratios of 0.7069–0.7076. Group 2 samples display high $^{87}Rb/^{86}Sr$ ratios (37.3–101.1) and high measured $^{87}Sr/^{86}Sr$ ratios (0.72449–0.76626), yielding unreasonable initial Sr isotopic ratios as low as 0.6963 (Table S3). Such high ratios are intrinsically linked to low Sr (as low as 20 ppm) at the time of magma solidification. As a result, the present-day Sr in the samples is largely radiogenic (i.e., ^{87}Sr), consequently resulting in variably elevated $^{87}Sr/^{86}Sr$ ratios. In this case, such unreasonable isotopic ratios have less petrogenetic significance and thus will not be considered in later discussions.

Group 1 samples show a limited range of whole-rock $\varepsilon_{Nd}(t)$ (-5.9 to -6.0) and a narrow range of two-stage Nd model ages (T_{DM2} = 1.33–1.35 Ga). These samples have whole-rock $\varepsilon_{Hf}(t)$ ranging from -4.0 to -4.5, and Hf isotope crustal model ages (T_{DM}^{C}) of 1.36–1.40 Ga, identical to the T_{DM2} model ages. The radiogenic Pb isotopic ratios of these samples are similar (i.e., $(^{206}Pb/^{204}Pb)i$ = 18.63–18.67, $(^{207}Pb/^{204}Pb)i$ = 15.72–15.74, $(^{208}Pb/^{204}Pb)i$ = 39.07–39.16) (Figs. 7a-c). Similar isotopic compositions are also observed in the Group 2 samples, including whole-rock $\varepsilon_{Nd}(t)$ (-5.7 to -6.7) and the corresponding T_{DM2} model ages (1.32–1.40 Ga) and whole-rock $\varepsilon_{Hf}(t)$ (-3.5 to -2.9) and the corresponding T_{DM}^{C} model ages (1.29–1.32 Ga). Compared to the Group 1 samples, the Group 2 samples display similar initial $^{207}Pb/^{204}Pb$ (15.71–15.73) and $^{208}Pb/^{204}Pb$ (39.14–39.28) but varying $^{206}Pb/^{204}Pb$ values (18.52–18.99) (Figs. 7a-c).

3.4. Zircon Hf isotopic data

In-situ zircon Hf isotopic analytical methods are provided in Appendix A, and the zircon Hf isotope data are listed in Table S4.

With the exception of one analysis that yields positive $\varepsilon_{Hf}(t)$ of +4.5, the other 14 analyses from sample 12DJC12-1 give $\varepsilon_{Hf}(t)$ of -2.4 to +0.4, corresponding to crustal model ages (T_{DM}^{C}) of 1.06–1.24 Ga. One analysis from sample 12DJC13-2 yields positive $\varepsilon_{Hf}(t)$ of +5.8 and a younger T_{DM}^{C} model age of 0.72 Ga, whereas the

remaining 11 analyses show $\varepsilon_{Hf}(t)$ of -4.3 to +2.2, yielding T_{DM}^{C} model ages of 0.95–1.36 Ga. Analyses of 18 zircons from sample 12DJC14-2 give $\varepsilon_{Hf}(t)$ of −6.0 to +1.3, yielding T_{DM}^{C} model ages ranging from 1.01 to 1.48 Ga.

These data indicate that the three samples from Group 1 display coherent zircon $\varepsilon_{Hf}(t)$ (Figs. 8a-b), indistinguishable within analytical error to those of a syenogranite sample (08CQ02) from Group 2 (-2.0 to +4.2; Zhu et al., 2011) (Figs. 8a and 8c), suggesting that the samples of the two groups originated from a common source region.

4. Discussion

4.1. Magmatism at ca. 43 ± 3 Ma in the Gangdese Batholith

The geochronological data reported here, along with the data of Zhu et al. (2011), indicate that the two petrogenetic groups of the Dajia pluton, western Gangdese Batholith, were emplaced synchronously at ca. 43 Ma. Coeval felsic granitoid rocks have also been documented by the zircon U-Pb method from the central and eastern Gangdese Batholith (Fig. 1b), including from east to central Bayi (44.3 ± 0.8 Ma; Ji, 2010), Wolong (37.4 ± 0.2 Ma; Guan et al., 2012), Cuijiu (42 ± 0.7 Ma; Ji et al., 2012), Sangri (ca. 45-37 Ma, Ji et al., 2012; 42.5 ± 0.5 Ma, Harrison et al., 2000), Lhasa (46.4 ± 0.8 Ma; Xu, 2010), Quxu (41.9–44 Ma, Ji et al., 2009; 40.5 ± 0.5 Ma, Xu, 2010; 46.4 ± 1 Ma, Wen et al., 2008a), Nyimu (46.7 ± 0.7 Ma, Xu, 2010), Namling (ca. 45 Ma, Cong et al., 2012; 40.7 ± 0.5 Ma, Xu, 2010), and Xaitongmoin (45.1 ± 1.7 Ma, Xia et al., 2008; 46.5 ± 1.1 Ma, Tang et al., 2010). Coeval intermediate dioritic rocks from Wolong (38.5 ± 0.3 Ma; Guan et al., 2012) in the east, Lhasa (43.4 ± 1 Ma; Xu, 2010) and Renbu (45 ± 1.6 Ma; Huang et al., 2010) and gabbros from Quxu (46.2 ± 1.5 Ma; Jia, 2014) and Nyimu (46.5 ± 1 Ma; Jia, 2014) in the center of the Gangdese Batholith are also reported. In the western Gangdese Batholith (Fig. 1b), several studies documented the presence of coeval gabbro (44.8 Ma) from Amuxiong (our unpublished data), monzogranite from Kangrinboqê (42.5 ± 0.5 Ma, Dong, 2008), and gabbro (ca. 45.5 Ma), diorite (46.7 ± 2.9 Ma), and granite (46.1 ± 0.8 Ma) from Namuru (Dong et al., 2011).

These available zircon U-Pb age data for varying lithologies suggest that (1) the 43 ± 3 Ma magmatism extends along the entire 1500 km strike length of the Gangdese

Batholith and (2) the magmatism is dominated by felsic compositions (Fig. 9). Fig. 1b reveals that this phase of magmatism is largely restricted to the southern edge of the Gangdese Batholith. This phase of magmatism represents the waning stage of magmatic activity following the flare-up ca. 52 Ma (cf. Zhu et al., 2015) within the Gangdese arc.

4.2. Rock type: Moderately vs. strongly fractionated granites

The subdivision of the Dajia pluton into moderately and strongly fractionated groups is also indicated by geochemical criteria. The moderately fractionated samples (Group 1) are characterized by low (Na_2O+K_2O)/CaO ratios (4.34–14.80) (except sample 12DJC13-2 with 28.8), low FeO*/MgO of 2.86–4.07 (except sample 12DJC13-2 with 26.8), and high Zr+Nb+Ce+Y abundances (344.5–483.6 ppm), whereas the strongly fractionated samples (Group 2) show enhanced (Na_2O+K_2O)/CaO ratios (18.35–47.33) and FeO*/MgO (4.33–27.85), and low Zr+Nb+Ce+Y abundances (172.6–253.2 ppm) for the Group 2 samples (Figs. 10a-b). Although samples 12DJC13-2 and 12DJC16-2 plot within the field of A-type granite (Whalen et al., 1987), the Dajia samples cannot be considered as A-type granite because these two samples have very low MgO (0.08 wt.% and 0.02 wt.%, respectively) due to strong fractionation of biotite (see below), and the remaining samples are highly or moderately fractionated.

It is difficult to identify the petrogenetic type of fractionated granites because such rocks tend to display converging major element and mineral compositions to haplogranite (King et al., 1997; Wu et al., 2007). In this case, the relationship between P_2O_5 and SiO_2 is generally considered as a proxy to determine the petrogenetic type of granites (Chappell, 1999; Wu et al. 2003; Li et al., 2007). This is because the P_2O_5 abundances will reduce in fractionated I-type granites as apatite reaches saturation in metaluminous and mildly peraluminous magmas (Montel et al., 1988; Chappell, 1999; Li et al., 2007). Thus, the negative trend of Group 1 and Group 2 samples on the P_2O_5 vs. SiO_2 plot (Fig. 5d), together with the absence of minerals that generally occur in S-type granites (e.g., muscovite), suggests an affinity to I-type granite in the Dajia pluton (Chappell, 1999; Wu et al. 2003; Li et al., 2007). However, the majority Group 1 and Group 2 samples display high A/CNK ratios, over 1.1, which indicate an affinity to S-type granite (cf. Chappell and White, 2001). Nevertheless, we consider

that the Dajia samples are not S-type because such high ratios probably resulted from the strong fractionation of feldspar that leads to a significant decrease in CaO (Fig. 5c).

4.3. Petrogenesis

4.3.1. Moderately fractionated granites (Group 1)

To account for the petrogenesis of the moderately fractionated calc-alkaline I-type granites, several models have been developed: (1) advanced assimilation and fractional crystallization of mantle-derived basaltic parental magmas (Bacon and Druitt, 1988; Grove et al., 1997; Beard and Lofgren, 1991; Sisson et al., 2005), (2) partial melting of mafic to intermediate meta-igneous crustal rocks with or without addition of mantle-derived mafic magmas (Petford and Atherton, 1996; Chappell and Stephens, 1988; Chappell and White, 2001; Li et al., 2007), and (3) reworking of supracrustal materials by juvenile magmas (Kemp et al., 2007; Collins and Richards, 2008). It has been shown that the rocks produced by fractional crystallization from mafic liquids generally show a wide range in composition and inflexions of elements on variation diagrams, including the occurrence of abundant cumulate rocks (cf. Keller et al., 2015), as exemplified by the I-type Boggy Plain Supersuite granites from the Lachlan Fold Belt (Chappell, 1999) and the Cordillera arc in the North American margin (cf. Lee et al., 2007). However, this is not the case for the Dajia pluton, which is exclusively felsic without mafic to intermediate varieties. Furthermore, in a regional context, the 43 ± 3 Ma magmatism along the Gangdese Batholith does not display a continuous gradation in SiO_2 (with a gap at 57–59 wt.%) and is dominated by felsic compositions (Fig. 9), with rare occurrence of mafic rocks and cumulates, precluding the possibility that the Dajia samples were generated by fractional crystallization of mantle-derived basaltic parental magmas. It is also unlikely that the reworking of supracrustal materials with varying contributions from mantle-derived magmas (Kemp et al., 2007; Collins and Richards, 2008) can account for the petrogenesis of Group 1 samples because this mechanism will produce zircons with a wide range of $\varepsilon_{Hf}(t)$ values (up to 10-ε units) within a single rock sample (e.g., Kemp et al., 2007), which is not the case for the Group 1 samples.

The samples in Group 1 have negative whole-rock $\varepsilon_{Nd}(t)$ values of -5.9 to -6.0 (T_{DM2} = 1.33–1.35 Ga) and $\varepsilon_{Hf}(t)$ values of -4.0 – -4.5 (T_{DM}^{C} = 1.36–1.40 Ga), which

suggest a Mesoproterozoic crustal source. However, we consider this to be unlikely because the southern Lhasa subterrane is characterized by the presence of a juvenile crust; partial melting of such crust will produce magmas (i.e., the Gangdese Batholith) showing mantle-type whole-rock $\varepsilon_{Nd}(t)$ (mostly > 3) and zircon $\varepsilon_{Hf}(t)$ (mostly 5–10) (Chung et al., 2005; Chu et al., 2006; Ji et al., 2009; Zhu et al., 2011). It should be noted that the Group 1 samples show the lowest zircon $\varepsilon_{Hf}(t)$ compared to granitoids from the Gangdese Batholith (including the ca. 50 Ma granites from approximately 17 km north of Dajia) (Fig. 8a), indicating that an exotic, isotopically enriched component has been involved in the generation of the Group 1 samples.

Two possibilities can be considered to account for the involvement of such an isotopically enriched component. The first involves the contributions from the subducting ancient Indian continental crust, as the Dajia pluton is exposed approximately 15 km north of the Indus–Yarlung-Zangbo suture zone (Fig. 1b), and the Indian continental crust may have already been subducted to depths when the Dajia pluton was emplaced (cf. Leech et al., 2005; Chu et al., 2011; Zhu et al., 2015). This interpretation is supported by the Nd-Hf-Pb isotopic compositions of the Dajia granitoids. Taking the Gangdese mafic lower crust, represented by a gabbro sample (Wen et al., 2008b), and the Indian continental crust, represented by Himalayan sedimentary rocks with very low Hf and Nd isotopic ratios (Chauvel et al., 2008), as two end members, the results of binary mixing indicate that mixing approximately 40 % Himalayan sediments into the mafic lower crust source can generate the Nd-Hf isotopic compositions of the Dajia pluton (Fig. 7a). The Pb isotopic compositions of the Group 1 samples further corroborate the involvement of Indian continental crust materials as these samples straddle the fields between the Himalayan basement (Gariépy et al., 1985; Schärer et al., 1986) and the central Lhasa subterrane basement-derived melts (Gariépy et al., 1985; Liao, 2003) (Figs. 7b-c).

The second possibility responsible for the enriched component documented by the Group 1 samples is the involvement of materials from the central Lhasa subterrane with ancient basement, as exemplified by the Miocene ultrapotassic rocks (cf. Liu et al., 2014). The first mechanism cannot explain why the coeval gabbro (44.8 Ma, our unpublished data) from Amuxiong, approximately 50 km east of Dajia, shows large positive zircon $\varepsilon_{Hf}(t)$ (mostly +5 to +10) (Fig. 8a) rather than small positive to negative zircon $\varepsilon_{Hf}(t)$, as expected for the involvement of the subducting Indian

continental material. Quantitative modeling shows that the whole-rock Nd-Hf isotopic compositions of the Group 1 samples can be interpreted as the result of mixing between juvenile Gangdese lower crust-derived melts (Wen et al., 2008b) and approximately 30% ancient basement-derived melts represented by the strongly peraluminous S-type granitic melts (Zhu et al., 2011) from the central Lhasa subterrane (Fig. 7a). The Pb isotopic compositions of the Group 1 samples that straddle the fields between the Himalayan basement (Gariépy et al., 1985; Schärer et al., 1986) and the central Lhasa subterrane basement-derived melts (Gariépy et al., 1985; Liao, 2003) (Figs. 7b-c) suggest the possible involvement of the central Lhasa basement-derived melts in their generation.

The moderately fractionated (DI = 84–93) nature of the Group 1 samples indicates that their compositions are closer to those of their parental magmas relative to the Group 2 samples, and thus, the least fractionated sample (12DJC13-1) with 68.66 wt.% SiO_2 and La/Yb ratio of 26.8 in Group 1 can be considered to record the nature of the magma source region. This sample, as well as the remaining Group 1 samples, shows fractionated REE patterns ($(La/Yb)_N$ = 18.1–26.9) and low Yb (≤ 2 ppm) and Y (≤ 19 ppm) abundances, suggesting derivation from a mafic source region, with garnet as a residual phase (cf. Rapp et al., 1991). Among the middle to HREEs, Yb and Lu have the highest garnet-melt partition coefficients, whereas Dy and Ho have the highest hornblende-melt partition coefficients (cf. Rollinson, 1993). As a result, middle to heavy REEs will strongly fractionate when garnet is the main residual phase, whereas a flat or concave-upward middle to heavy REE pattern will be expected if amphibole is the main residual phase (Gromet and Silver, 1987). Therefore, the $(Ho/Yb)_N$ ratios of approximately 1.0 (0.8–1.1) of the Group 1 samples suggest amphibole is a dominant phase in the residue during partial melting.

In summary, Group 1 samples were most likely derived from partial melting of garnet-bearing amphibolite (rather than eclogite) within the juvenile southern Lhasa crust that mixed with enriched components from the subducting ancient Indian continental crust and/or the ancient central Lhasa basement.

4.3.2. Strongly fractionated granite (Group 2)

As shown in Fig. 6b, the Group 2 samples display significantly negative Ba, Sr, Nb, P, Ti, and Eu anomalies relative to the Group 1 samples, which could indicate the

involvement of supracrustal rocks in their generation. However, this possibility can be discarded because the Group 2 samples share a common magma source region with those of Group 1, as indicated by their similar Nd-Hf-Pb isotopes (Fig. 7). The evolved compositional trends defined by oxide contents (Fig. 5) of the two groups indicate that the Group 2 samples are most likely fractionated from melts represented by the Group 1 samples. Negative Nb, Ta, Ti, and P anomalies are commonly attributed to the fractionation of Ti-bearing phases (e.g., ilmenite and titanite) and apatite. Negative Eu depletions are related to extensive fractionation of plagioclase and/or K-feldspar (cf. Hanson, 1978). Generally, the positive correlation defined by Sr vs. Ba (Fig. 11a) and the negative correlation defined by Sr vs. Rb/Sr (Fig. 11b) are linked with K-feldspar fractionation. However, such correlations can also be interpreted as the consequences of fractional crystallization of plagioclase and biotite, which are consistent with the petrographical observations of the Group 2 samples that show more abundant K-feldspar megacrysts with minor plagioclase ± biotite relative to those of the Group 1 samples. For example, the Ba, Sr, and Rb abundances of the Group 2 samples can be quantitatively explained by 60–80% fractionation of 65% biotite and 35% plagioclase (Figs. 11a-b) starting from the assumed parent magma composition represented by the least fractionated sample (12DJC13-1) of Group 1.

Another distinct geochemical feature of the Dajia pluton is that the strongly fractionated Group 2 samples display lower REE abundances relative to the moderately fractionated Group 1 samples (Fig. 6a), which is opposite to that predicted from the fractionation trend. The REE abundances of granite are unrelated to the separation of feldspar and biotite (except for Eu) due to element incompatibility but are significantly controlled by the fractionation of accessory minerals (Ayres and Harris, 1997; Wu et al., 2003). Thus, the decreased REE abundances of the Group 2 samples are suggestive of the separation of accessory minerals, including apatite, titanite, allanite and monazite (Fig. 11c). Quantitative modeling reveals that the REE abundances (except for Eu) of the Group 2 samples can be generated by 1–3% fractional crystallization of 2% titanite, 4% allanite, and 94% apatite from the assumed starting compositions (12DJC13-1) (Fig. 12). The modeling results also show that the fractional crystallization of these accessory minerals is capable of causing the decrease in middle REEs abundances, explaining the concave-upward middle REE patterns of this group (Fig. 6a). This explanation is also supported by the

absence of a negative trend between SiO_2 and Sc (Fig. 5e), which is expected in hornblende controlled fractionation (Davidson et al., 2007).

In summary, the Group 2 samples were most likely derived from the melts represented by the Group 1 samples through fractional crystallization of plagioclase, K-feldspar, biotite, apatite, allanite, titanite, monazite, and ilmenite.

4.4. Implications for crustal thickening and magma generation

It is well-known that the Central Andes has a crustal thickness of approximately 70 km (Wigger et al., 1994; Zandt et al., 1994), which is similar to that in southern Tibet. Geochemical and isotopic data of modern Andean magmatic arc rocks have been considered as strong proxies to explore the history of crustal thickening through time (e.g., Kay et al., 1987, 1991; Trumbull et al., 1999). This is because crustal thickening will result in changing mineral assemblages within the source regions from lower-pressure assemblages dominated by plagioclase and clinopyroxene to higher-pressure assemblages characterized by amphibole and garnet, producing melts with distinct geochemical signatures (e.g., more enriched in K, strongly fractionated REE patterns, low HREEs abundances, and high Sr/Y ratios) (e.g., Kay et al., 1987; Drummond and Defant, 1990; Haschke et al., 2002). Similar studies have also been conducted in the central and eastern Gangdese Batholith and provide varying ages of crustal thickening, ranging from 62 Ma to 25 Ma (Mo et al., 2007; Chung et al., 2009; Guan et al., 2012; Ji et al., 2012; Jiang et al., 2014). For example, the presence of the Linzizong high-K calc-alkaline to shoshonitic volcanic rocks likely indicates that the crust immediately north of the Gangdese Batholith may have been thickened at ca. 50–40 Ma (Mo et al., 2007). On the basis of the identification of the earliest adakitic rocks with low HREEs abundances and high Sr/Y ratios, which indicate the presence of garnet as a residual phase in the source, several studies proposed that the central to eastern Gangdese crust has been thickened to > 50 km prior to ca. 30 Ma (Chung et al., 2009), ca. 38 Ma (Guan et al., 2012), ca. 51 Ma (Ji et al., 2012), and ca. 62 Ma (Jiang et al., 2014).

Although the Dajia pluton does not show adakitic signatures as indicated by the low Sr abundances and Sr/Y ratios, which most likely resulted from the extensive fractionation of plagioclase, their low HREEs and Y abundances suggest the presence of garnet as a residual phase in the source (cf. Rapp et al., 1991). This indicates that

the Gangdese crust beneath the Dajia region had already been thickened (cf. Rapp et al., 1991) when the Dajia pluton was emplaced (ca. 43 Ma). Further evidence for this conclusion comes from the presence of the Dajia strongly fractionated granites (Group 2), which was identified for the first time in this study. This is because if the juvenile Gangdese crust was not thickened by ca. 43 Ma, melts are difficult to stagnate in the crust, thereby discouraging fractionation (Pearcy et al., 1990; Miller and Christensen, 1994), which is inconsistent with the presence of the Group 2 samples. In contrast, if the juvenile Gangdese crust had already been thickened at that time, the melts would stagnate in the crust, thereby encouraging extensive fractionation (Hildreth and Moorbath, 1988; Stern, 2002) to form the Group 2 samples.

The observations and interpretations presented above corroborate that the Gangdese crust, not only the central to eastern portions but also the western segment, was thickened by ca. 43 Ma. Importantly, the Gangdese crustal thickening was coeval with the Tethyan Himalaya crustal thickening, as revealed by the structural geology (Aikman et al., 2008) and geochemistry of the Dala and Yardoi adakitic granites (ca. 43 Ma) (Zeng et al., 2011; Hou et al., 2012). This indicates that the crust on both sides of the Yarlung Zangbo suture zone was thickened by ca. 43 Ma. In this case, a distinct deep process is required to explain the generation of such coeval magmatism that left garnet in the residual phase in the source. This is because normal geothermal gradients are insufficient to provide the heat required for partial melting of the thickened crust (cf. Sandiford et al., 1998). This is true for the Group 1 samples that yield high whole-rock zircon saturation temperatures (815°C–869°C) (Watson and Harrison, 1983), suggesting a mantle-derived heat supply for their generation.

The voluminous Linzizong volcanic succession and coeval granitoids with abundant mafic enclaves within the Gangdese Batholith have previously been attributed to the breakoff of the Neo-Tethyan Ocean slab at ca. 50 Ma (Wen et al., 2008a; Chung et al., 2009; Ji et al., 2009; Lee et al., 2009, 2012; Zhu et al., 2011). A recent comprehensive synthesis of geological, geochronological, and geochemical data reveals the presence of magmatic flare-up at ca. 52–51 Ma, which is attributed to the breakoff of the Neo-Tethyan oceanic lithosphere at ca. 53 Ma (Fig. 13a; Zhu et al., 2015). Thermo-mechanical modeling shows that the slab breakoff can significantly increase the temperature in the overlying lithosphere due to the upwelling of hot asthenosphere through the slab window. As a consequence, partial melting of the

asthenosphere and the overriding metasomatized lithosphere will produce mafic magmatism for a few million years and crustal anatexis to generate crust-derived magmatism over a considerably longer period (van de Zedde and Wortel, 2001). In this case, the ca. 43 Ma magmatism documented both in the Gangdese Batholith (including the Dajia pluton reported in this study) (Fig. 1b) and in the Tethyan Himalaya can best be interpreted as the consequence of the slab breakoff of the Neo-Tethyan oceanic lithosphere (Fig. 13b). This favored slab breakoff model is further corroborated by a recent identification of ca. 45 Ma OIB-type magmatism from Langshan immediately to the south of the Yarlung Zangbo suture zone (Ji et al., in preparation).

5. Conclusions

(1) The Dajia pluton in the western Gangdese Batholith includes moderately (Group 1) and strongly (Group 2) fractionated granites that were emplaced synchronously at ca. 43 Ma.

(2) The Group 1 samples display varying SiO_2 (69–72 wt.%) and differentiation index values (DI = 84–93) and low HREEs and Y contents. The Group 2 samples are characterized by high SiO_2 (75–78 wt.%) and DI (95–97) and significantly negative Ba, Sr, P, and Ti anomalies. The Group 1 and Group 2 samples have similar zircon $\varepsilon_{Hf}(t)$ values and whole-rock Nd-Hf-Pb isotopic compositions.

(3) The Group 1 samples are interpreted as being the products of partial melting of garnet-bearing amphibolite within the juvenile southern Lhasa crust that mixed with enriched components (from the subducting ancient Indian continental crust and/or the ancient central Lhasa basement). The Group 2 samples were most likely derived from the melts represented by the Group 1 samples through extensive fractional crystallization of plagioclase, K-feldspar, biotite, apatite, allanite, titanite, monazite, and ilmenite.

(4) The Dajia pluton provides robust geochemical and petrological evidence for crustal thickening of the southern Lhasa Terrane by ca. 43 Ma.

Acknowledgements

This research was financially co-supported by the Strategic Priority Research

Program (B) of the Chinese Academy of Sciences (XDB03010301), the National Key Project for Basic Research of China (Project 2015CB452604), the Chinese National Natural Science Foundation (41225006, 41472061, and 40973026), the MOST Special Fund from the State Key Laboratory of Geological Processes and Mineral Resources (China University of Geosciences). The first author thanks the China Scholarship Council (201306400021). We thank two anonymous reviewers for constructive comments that have improved the quality of this paper and Editor Andrew Kerr for comments and editorial handling.

Appendix A. Descriptions of analytical methods

LA-ICP-MS zircon U-Pb dating

In this study two monzogranite samples (12DJC13-2 and 12DJC14-2) and one syenogranite sample (12DJC12-1) were selected for *in situ* zircon U-Pb and Hf isotope analysis. Zircons were separated for each sample by heavy-liquid and magnetic methods in the Laboratory of the Geological Team of Hebei Province, China. Cathodoluminescence (CL) images were taken at the Institute of Geology, Chinese Academy of Geological Sciences (Beijing) to inspect internal structures of individual zircons and to select positions for zircon isotope analyses. Zircon U-Pb dating with a beam size of 32 μm was conducted by laser ablation-inductively coupled plasma mass spectrometry (LA-ICPMS) at the State Key Laboratory of Geological Processes and Mineral Resources, China University of Geosciences (Wuhan). The detailed operating conditions for the laser ablation system, the ICP-MS instrument and data reduction are the same as those described by Liu et al. (2010). Off-line selection and the integration of background and analyse signals, time-drift correction, U-Pb dating, and quantitative calibration for trace element analyses were performed by *ICPMSDataCal* (Liu et al., 2010). Trace element compositions of zircons were calibrated against multiple-reference materials (BCR-2G and BIR-1G) combined with internal standardization (Liu et al., 2010). The common Pb correction followed the ComPbCorr#3-151 procedure (Andersen, 2002). ISOPLOT (version 3.0) (Ludwig, 2003) was used to plot concordia diagrams and for age calculations. Uncertainties of individual analyses are reported as 1σ (Table S1); mean ages for pooled $^{206}Pb/^{238}U$ results are reported as 2σ (Fig. 3).

Major and trace elements, and whole-rock Sr-Nd-Pb-Hf isotopic analysis

Whole-rock samples were crushed, hand-picked, and then powdered using a jaw crusher and a corundum mill. Concentrations of major elements were determined by the X-ray fluorescence (XRF) method using a Rigaku® RIX 2000 spectrometer at the Department of Geosciences, National Taiwan University. The analytical uncertainties are generally better than 5% for all elements (Yang et al., 2005). Loss on ignition (LOI) was determined by routine procedures. Trace elements were measured by

inductively coupled plasma-mass spectrometry (ICP-MS) using an Agilent® 7500cx spectrometer also in the Department of Geosciences, National Taiwan University, which shows a good stability range within ~5% variation. Powder samples weighing ~20 mg were dissolved in screw-top Teflon beakers using super-pure HF and HNO_3 (1:1) mixture for 7–10 days at ~100°C, followed by evaporation to dryness, refluxing in HF and HNO_3 (1:1) mixture for >12 h at ~100°C and drying again, and then dissolving the sample cake in 2% HNO_3. An internal standard solution of 10 ppb Rh and Bi was added and the spiked dissolutions were diluted with 2% HNO_3 to a sample/solution weight ratio of 1/4000. The analytical accuracy and precision are generally better than 3%. During analysis, data quality was monitored by repeated analyses of USGS rock reference materials (AGV-2, BHVO-2, and BCR-2) (see Table S5). Detailed analytical information has been reported in Lin et al. (2012).

The whole-rock Sr-Nd-Pb-Hf isotopic analyses of Dajia pluton were performed at Washington State University using a Thermo Finnigan multi-collector-inductively coupled plasma mass spectrometer (MC-ICPMS). For whole-rock Sr isotope analysis, measured $^{87}Sr/^{86}Sr$ were normalized to $^{86}Sr/^{88}Sr = 0.1194$ for mass fractionation correction. During the period of data acquisition, the mean $^{87}Sr/^{86}Sr$ ratio of NBS987 standard was 0.710239 ± 31 (n = 12). For whole-rock Nd and Hf isotope analysis, elemental concentrations of Lu, Hf, Sm, and Nd as well as parent/daughter ratios ($^{176}Lu/^{177}Hf$ and $^{147}Sm/^{144}Nd$) were determined by isotope dilution on the same solution as the isotope composition measurements. Mass bias corrections on Hf, Nd, and Sm were made with the exponential law and using $^{179}Hf/^{177}Hf = 0.7325$, $^{146}Nd/^{144}Nd = 0.7219$, and $^{147}Sm/^{152}Sm = 0.56081$. Mass bias corrections on the $^{176}Lu/^{175}Lu$ ratio are based on $^{173}Yb/^{171}Yb$ using natural Yb left in the sample following the method outlined in Vervoort et al. (2004). Final values for $^{176}Hf/^{177}Hf$ and $^{143}Nd/^{144}Nd$ were adjusted relative to $^{176}Hf/^{177}Hf = 0.282141$ (n = 6) for the JMC475 Hf standard and $^{143}Nd/^{144}Nd = 0.511822$ (n = 6) for the LaJolla Nd standard. Detailed analytical information of whole-rock Nd and Hf isotopic analysis were given in Vervoort et al. (2011). For Pb isotopic analysis, Tl ($^{205}Tl/^{203}Tl = 2.388$) was used to correct for mass bias (White et al., 2000). Final Pb isotope values were normalized relative to the values for NBS981 of Galer and Abouchami (1998). The average values and associated errors (2σ) of Pb isotope standard NBS981 in this study were: $^{206}Pb/^{204}Pb = 16.9346 \pm 0.0020$ (n = 8), $^{207}Pb/^{204}Pb = 15.4908 \pm 0.0018$ (n = 8), and

$^{208}Pb/^{204}Pb = 36.6978 \pm 0.0038$ (n = 8) for multiple analytical sessions. All initial isotopic ratios are corrected to t = 43 Ma.

Zircon Hf isotopic analysis

In situ Hf isotope measurements were conducted on the dated spots within the zircons using a Thermo Finnigan Neptune sector multi-collector-ICPMS and a Geolas CQ 193 nm laser ablation system housed at Department of Geosciences, National Taiwan University. Details of instrumental conditions and data acquisition were given in Wu et al. (2006). During the analysis, $^{176}Hf/^{177}Hf$ ratios of the zircon standard (91500) were 0.282286 ± 12 ($2\sigma_n$, n = 21). Initial $^{176}Hf/^{177}Hf$ ratios and $\varepsilon_{Hf(t)}$ values were calculated with the reference to the chondritic reservoir (CHUR) at the time of zircon growth from magmas, the chondritic $^{176}Hf/^{177}Hf$ ratio of 0.282785 and $^{176}Lu/^{177}Hf$ ratio of 0.0336 are from Bouvier et al. (2008). Depleted mantle model ages (T_{DM}) were calculated with reference to the depleted mantle at a present-day $^{176}Hf/^{177}Hf$ ratio of 0.28325, and $^{176}Lu/^{177}Hf = 0.0384$ (Griffin et al., 2000). Crustal model ages (T_{DM}^{C}) were calculated assuming a $^{176}Lu/^{177}Hf = 0.015$ for the average continental crust (Griffin et al., 2002).

References

Aikman, A.B., Harrison, T.M., Ding, L., 2008. Evidence for Early (> 44 Ma) Himalayan crustal thickening, Tethyan Himalaya, southeastern Tibet. Earth and Planetary Science Letters 274, 14–23.

Andersen, T., 2002. Correction of common lead in U–Pb analyses that do not report ^{204}Pb. Chemical Geology 192, 59–79.

Ayres, M., Harris, N., 1997. REE fractionation and Nd-isotope disequilibrium during crustal anatexis: constraints from Himalayan leucogranites. Chemical Geology, 139, 249–269.

Bacon, C., Druitt, T., 1988. Compositional evolution of the zoned calcalkaline magma chamber of Mount Mazama, Crater Lake, Oregon. Contributions to Mineralogy and Petrology 98, 224–256.

Beard, J.S., Lofgren, G.E., 1991. Dehydration melting and water-saturated melting of basaltic and andesitic greenstones and amphibolites at 1, 3, and 6. 9 kb. Journal of Petrology 32, 365–401.

Bouvier, A.,Vervoort, J.D., Patchett, P.J., 2008. The Lu-Hf and Sm-Nd isotopic composition of CHUR: constraints from unequilibrated chondrites and implications for the bulk composition of terrestrial planets. Earth and Planetary Science Letters 273, 48–57.

Chappell, B.W., 1999. Aluminium saturation in I- and S-type granites and the characterization of fractionated haplogranites. Lithos 46, 535–551.

Chappell, B.W., Stephens, W.E., 1988. Origin of infracrustal (I-type) granite magmas. Transactions of the Royal Society of Edinburgh: Earth Sciences 79, 71–86.

Chappell, B.W., White, A.J.R., 2001. Two contrasting granite types: 25 years later. Australian Journal of Earth Sciences 48, 489–499.

Chauvel, C., Lewin, E., Carpentier, M., Arndt, N.T., Marini, J.C., 2008. Role of recycled oceanic basalt and sediment in generating the Hf–Nd mantle array. Nature Geoscience 1, 64–67.

Chu, M.F., Chung, S.L., O'Reilly, S.Y., Pearson, N.J., Wu, F.Y., Li, X.H., Ji, J.Q., Liu, D.Y., Ji, J.Q., Chu, C.H., Lee, H.Y., 2011. India's hidden inputs to Tibetan orogeny revealed by Hf isotopes of Transhimalayan zircons and host rocks. Earth and Planetary Science Letters 307, 479–486.

Chu, M.F., Chung, S.L., Song, B., Liu, D.Y., O'Reilly, S.Y., Pearson, N.J., Ji, J.Q., Wen, D.R., 2006. Zircon U–Pb and Hf isotope constraints on the Mesozoic tectonics and crustal evolution of Southern Tibet. Geology 34, 745–748.

Chung, S.L., Chu, M.F., Ji, J.Q., O'Reilly, S.Y., Pearson, N.J., Liu, D.Y., Lee, T.Y., Lo, C.H., 2009. The nature and timing of crustal thickening in Southern Tibet: Geochemical and zircon Hf isotopic constraints from postcollisional adakites. Tectonophysics 477, 36–48.

Chung, S.L., Chu, M.F., Zhang, Y.Q., Xie, Y.W., Lo, C.H., Lee, T.Y., Lan, C.Y., Li, X.H., Zhang, Q., Wang, Y.Z., 2005. Tibetan tectonic evolution inferred from spatial and temporal variations in post-collisional magmatism. Earth-Science Reviews 68, 173–196.

Chung, S.L., Liu, D.Y., Ji, J.Q., Chu, M.F., Lee, H.Y., Wen, D.J., Lo, C.H., Lee, T.Y., Qian, Q., Zhang, Q., 2003. Adakites from continental collision zones: melting of thickened lower crust beneath southern Tibet. Geology 31, 1021–1024.

Collins, W.J., Richards, S.W., 2008. Geodynamic significance of S-type granites in circum-Pacific orogens. Geology 36, 559–562.

Cong, Y., Xiao, K.Y., Zhai, Q.G., Dong, Q.J., 2012. LA-ICP-MS dating and Hf isotopic analysis of zircon from the Puluogang granite in Namulin County, Tibet, and its geological significance. Journal of Jilin University 42, 1783–1795 (in Chinese with English abstract).

Davidson, J., Turner, S., Handley, H., Macpherson, C., Dosseto, A., 2007. Amphibole "sponge" in arc crust? Geology 35, 787–790.

Dong, G.C., Mo, X.X., Zhao, Z.D., Zhu, D.C., Xie, X.F., Dong, M.L., 2011. The Neocene magmatism from Namuru intrusion in western Gangdese, Tibet and its tectonic significance. Acta Petrologica Sinica 27, 1983–1992 (in Chinese with English abstract).

Dong, X., 2008. The geochronology and geochemistry of the Mesozoic and Cenozoic granitoids from southwestern Gangdese belt, Tibet. Unpublished result. MS thesis, China University of Geosciences (Beijing).

Drummond, M.S., Defant, M.J., 1990. A model for trondhjemite-tonalite-dacite genesis and crustal growth via slab melting: Archean to modern comparisons. Journal of Geophysical Research 95, 21503–21521.

Dong, X., Zhang, Z.M., Santosh, M., 2010. Zircon U-Pb Chronology of the Nyingtri Group, Southern Lhasa Terrane, Tibetan Plateau: Implications for Grenvillian and Pan-African Provenance and Mesozoic–Cenozoic Metamorphism. Journal of Geology 118, 677–690.

Deng, J., Wang, Q.F., Li, G.J., Li, C.S., Wang, C.M., 2014. Tethys tectonic evolution and its bearing on the distribution of important mineral deposits in the Sanjiang region, SW China. Gondwana Research 26, 419–437.

De la Roche, H., Leterrier, J., Grande Claude, P., Marchal, M., 1980. A classification of volcanic and plutonic rocks using R1–R2 diagrams and major element analyses—its relationship and current nomenclature. Chemical Geology 29, 183–210.

Galer, S.J.G., Abouchami, W., 1998. Practical application of lead triple spiking for correction of instrumental mass discrimination. Mineralogical Magazine 62A, 491–492.

Gariépy, C., Allègre, C.J., Xu, R.H., 1985. The Pb-isotope geochemistry of granitoids from the Himalaya-Tibet collision zone: implications for crustal evolution. Earth and Planetary Science Letters 74, 220–234.

Green, T.H., Pearson, N.J., 1986. Rare-earth element partitioning between titanite and coexisting silicate liquid at high pressure and temperature. Chemical Geology 55, 105–119.

Griffin, W.L., Pearson, N.J., Belousova, E., Jackson, S.E., van Achterbergh, E., O'Reilly, S.Y., Shee, S.R., 2000. The Hf isotope composition of cratonic mantle: LAM-MC-ICPMS analysis of zircon megacrysts in kimberlites. Geochimica et Cosmochimica Acta 64, 133–147.

Griffin, W.L., Wang, X., Jackson, S.E., Pearson, N.J., O'Reilly, S.Y., Xu, X., Zhou, X., 2002, Zircon chemistry and magma mixing, SE China: In-situ analysis of Hf isotopes, Tonglu and Pingtan igneous complexes. Lithos 61, 237–269.

Gromet, L.P., Silver, L.T., 1987. REE variations across the Peninsular Ranges batholith: implications form batholith petrogenesis and crustal growth in magmatic arcs. Journal of Petrology 28, 75–125.

Grove, T.L., Donnelly-Nolan, J.M., Housh, T., 1997. Magmatic processes that generated the rhyolite of Glass Mountain, Medicine Lake volcano, N. California. Contributions to Mineralogy and Petrology 127, 205–223.

Guan, Q., Zhu, D.C., Zhao, Z.D., Dong, G.C., Zhang, L.L., Li, X.W., Liu, M., Mo, X.X., Liu, Y.S., Yuan, H.L., 2012. Crustal thickening prior to 38 Ma in southern Tibet: evidence from lower crust-derived adakitic magmatism in the Gangdese Batholith. Gondwana Research 21, 88–99.

Hanson, G.N., 1978. The application of trace elements to the petrogenesis of igneous rocks of granitic composition. Earth and Planetary Science Letters 38, 26–43.

Harrison, T.M., Yin, A., Grove, M., Lovera, O.M., Ryerson, F.J., Zhou, X., 2000. The Zedong Window: a record of superposed Tertiary convergence in southeastern Tibet. Journal of Geophysical Research 105, 19211–19230.

Hart, S.R., 1984. The DUPAL anomaly: a large-scale isotopic anomaly in the southern hemisphere. Nature 309, 753–756.

Haschke, M., Siebel, W., Günther, A., Scheuber, E., 2002. Repeated crustal thickening and recycling during the Andean orogeny in north Chile (21°–26°S). Journal of Geophysical Research 107, doi:10.1029/2001JB000328.

He, S.D., Kapp, P., DeCelles, P.G., Gehrels, G.E., Heizler, M., 2007. Cretaceous-Tertiary geology of the Gangdese Arc in the Linzhou area, southern Tibet, Tectonophysics 433, 15–37.

Hildreth, W., Moorbath, S., 1988. Crustal contributions to arc magmatism in the Andes of Central Chile. Contributions to Mineralogy and Petrology 98, 455–489.

Hoskin, P.W.O., Schaltegger, U., 2003. The composition of zircon and igneous and metamorphic petrogenesis. Reviews in Mineralogy and Geochemistry 53, 27–62.

Hou, Z.Q., Zheng, Y.C., Zeng, L.S., Gao, L.E., Huang, K.X., Li,W., Li, Q.Y., Fu, Q., Liang,W., Sun, Q.Z., 2012. Eocene–Oligocene granitoids in southern Tibet: constraints on crustal anatexis and tectonic evolution of the Himalayan orogen. Earth and Planetary Science Letters 349, 38–52.

Huang, Y., Zhao, Z.D., Zhang, F.Q., Zhu, D.C., Dong, G.C., Mo, X.X., 2010. Geochemistry and implication of the Gangdese batholiths from Renbu and Lhasa areas in southern Gangdese, Tibet. Acta Petrologica Sinica 26, 3131–3142 (in Chinese with English abstract).

Ji, W.Q., 2010. Geochronology and petrogenesis of granitic rocks from east segment of the Gangdese batholith, southern Tibet. Unpublished result. PhD thesis, Chinese Academy of Sciences.

Ji, W.Q., Wu, F.Y., Chung, S.L., Li, J.X., Liu, C.Z., 2009. Zircon U–Pb chronology and Hf isotopic constraints on the petrogenesis of Gangdese batholiths, southern Tibet. Chemical Geology 262, 229–245.

Ji, W.Q., Wu, F.Y., Chung, S.L., Wang, X.C., Liu, C.Z., Li, Q.L., Wang, J.G., Liu, X.C., in preparation. Eocene (45Ma) OIB-type magmatism in southern Tibet: First evidence for asthenospheric melting related to Neo-Tethyan slab breakoff.

Ji, W.Q., Wu, F.Y., Liu, C.Z., Chung, S.L., 2012. Early Eocene crustal thickening in southern Tibet: new age and geochemical constraints from the Gangdese batholith. Journal of Asian Earth Sciences 53, 82–95.

Jia, L.L., 2014. Regional variation of geochemical characteristics and tectonic implication of the Early Eocene basic rocks in southern Tibet. Unpublished result. MS thesis, China University of Geosciences (Beijing).

Jiang, Z.Q., Wang, Q., Wyman, D.A., Li, Z.X., Yang, J.H., Shi, X.B., Tang, G.J., Jia, X.H., Ma, L., Gou, G.N., Guo, H.F., 2014. Transition from oceanic to continental lithosphere subduction in southern Tibet: Evidence from the Late Cretaceous–Early Oligocene (~91–30 Ma) intrusive rocks in the Chanang–Zedong area, southern Gangdese. Lithos 196–197, 213–231.

Kapp, P., DeCelles, P.G., Leier, A.L., Fabijanic, J.M., He, S., Pullen, A., Gehrels, G.E., Ding, L., 2007. The Gangdese retroarc thrust belt revealed. GSA Today 17, doi:

10.1130/GSAT01707A.1.

Kapp, P., Murphy, M.A., Yin, A., Harrison, T.M., Ding, L., Guo, J.R., 2003. Mesozoic and Cenozoic tectonic evolution of the Shiquanhe area of western Tibet. Tectonics 22, 1029, doi: 10.1029/2001TC001332.

Kapp, P., Yin, A., Harrison, T.M., Ding, L., 2005. Cretaceous-Tertiary shortening, basin development, and volcanism in central Tibet. Geological Society of America Bulletin 117, 865–878.

Kay, S.M., Maksaev, V., Mpodozis, C., Moscoso, R., Nasi, C., 1987. Probing the evolving Andean lithosphere: Middle to late Tertiary magmatic rocks in Chile over the modern zone of subhorizontal subduction (29–31.5°S). Journal of Geophysical Research 92, 6173–6189.

Kay, S.M., Mpodozis, C., Ramos, V.A., Munizaga, F., 1991. Magma source variations for mid–late Tertiary magmatic rocks associated with a shallowing subduction zone and a thickening crust in the central Andes (28 to 33°S), in Harmon, R.S., and Rapela, C.W., eds., Andean magmatism and its tectonic setting. Geological Society of America Special Paper 265, 113–137.

Keller, C.B., Schoene, B., Barboni, M., Samperton, K.M., Husson, J.M., 2015. Volcanic–plutonic parity and the differentiation of the continental crust. Nature 523, 301–307.

Kemp, A.I.S., Hawkesworth, C.J., Foster, G.L., Paterson, B.A., Woodhead, J.D., Hergt, J.M., Gray, C.M., Whitehouse, M.J., 2007. Magmatic and crustal differentiation history of granitic rocks from Hf-O isotopes in zircon. Science 315, 980–983

King, P.L., White, A.J.R., Chappell, B.W., Allen, C.M., 1997. Characterization and origin of aluminous A-type granites from the Lachlan Fold Belt, Southeastern Australia. Journal of Petrology 38, 371–391.

Lee, C.T.A., Morton, D.M., Kistler, R.W., Bair, A.K., 2007. Petrology and tectonics of Phanerozoic continent formation: from island arcs to accretion and continental arc magmatism. Earth and Planetary Science Letters 263, 370–387.

Lee, H.Y., Chung, S.L., Ji, J.Q., Qian, Q., Gallet, S., Lo, C.H., Lee, T.Y., Zhang, Q., 2012. Geochemical and Sr-Nd isotopic constraints on the genesis of the Cenozoic Linzizong volcanic successions, southern Tibet. Journal of Asian Earth Sciences 53, 96–114.

Lee, H.Y., Chung, S.L., Lo, C.H., Ji, J.Q., Lee, T.Y., Qian, Q., Zhang, Q., 2009.

Eocene Neotethyan slab breakoff in southern Tibet inferred from the Linzizong volcanic record. Tectonophysics 477, 20–35.

Leech, M.L., Singh, S., Jain, A.K., Klemperer, S.L., Manichavasgam, R.M., 2005. The onset of India-Asia continental collision: Early, steep subduction required by the timing of UHP metamorphism in the western Himalaya. Earth and Planetary Science Letters 234, 83–97.

Li, X.H., Li, Z.X., Li, W.X., Liu, Y., Yuan, C.,Wei, G., Qi, C., 2007. U–Pb zircon, geochemical and Sr–Nd–Hf isotopic constraints on age and origin of Jurassic I- and A-type granites from central Guangdong, SE China: a major igneous event in response to foundering of a subducted flat-slab? Lithos 96, 186–204.

Liao, Z.L., 2003. Peraluminous Granites in Southern Tibet: Characteristics, Genesis and Tectonic Implications. Unpublished result. PhD thesis, China University of Geosciences (Beijing).

Lin, I.J., Chung, S.L., Chu, C.H., Lee, H.Y., Gallet, S., Wu, G., Ji, J., Zhang, Y., 2012. Geochemical and Sr–Nd isotopic characteristics of Cretaceous to Paleocene granitoids and volcanic rocks, SE Tibet: petrogenesis and tectonic implications. Journal of Asian Earth Sciences 53, 131–150.

Liu, D., Zhao, Z., Zhu, D-C., Niu, Y., DePaolo, D.J., Mark Harrison, T., Mo, X., Dong, G., Zhou, S., Sun, C., Zhang, Z., Liu, J., 2014. Postcollisional potassic and ultrapotassic rocks in southern Tibet: Mantle and crustal origins in response to India-Asia collision and convergence, Geochimica et Cosmochimica Acta 143, 207–231.

Liu, Y.S., Gao, S., Hu, Z.C., Gao, C.G., Zong, K.Q., Wang, D.B., 2010. Continental and oceanic crust recycling-inducedmelt-peridotite interactions in the trans-north China orogen: U–Pb dating, Hf isotopes and TRACE ELEMENTS IN ZIRCONS FROM MANTLE XENOLITHS. Journal of Petrology 51, 537–571.

Ludwig, K.R., 2003. Isoplot 3.00: a geochronological toolkit for Microsoft Excel. Special Publication No. 4. Berkeley Geochronology Center, pp. 1–70.

Mahood, G., Hildreth, W., 1983. Large partition coefficients for trace elements in high-silica rhyolites. Geochimica et Cosmochimica Acta 47, 11–30.

Miller, D. J., Christensen, N. I., 1994. Seismic signature and geochemistry of an island arc: A multidisciplinary study of the Kohistan accreted terrane, northern Pakistan. Journal of Geophysical Research 99, 11623–11642.

Mo, X., Dong, G., Zhao, Z., Zhu, D., Zhou, S., Niu, Y., 2009. Mantle Input to the

Crust in Gangdese, Tibet, during the Cenozoic: zircon Hf isotopic evidence. Journal of Earth Science 20, 241–249.

Mo, X.X., Dong, G.C., Zhao, Z.D., Zhou, S., Wang, L.L., Qiu, R.Z., Zhang, F.Q., 2005. Spatial and temporal distribution and characteristics of granitoids in the Gangdese, Tibet and implication for crustal growth and evolution (in Chinese with English abstract). Geological Journal of China Universities 11, 281–290.

Mo, X.X., Hou, Z.Q., Niu, Y.L., Dong, G.C., Qu, X.M., Zhao, Z.D., Yang, Z.M., 2007. Mantle contributions to crustal thickening during continental collision: evidence from Cenozoic igneous rocks in southern Tibet. Lithos 96, 225–242.

Mo, X.X., Niu, Y.L., Dong, G.C., Zhao, Z.D., Hou, Z.Q., Zhou, S., Ke, S., 2008. Contribution of syncollisional felsic magmatism to continental crust growth: A case study of the Paleogene Linzizong Volcanic Succession in southern Tibet. Chemical Geology 250, 49–68.

Montel, J.M., Mouchel, R., Pichavant, M., 1988. High apatite solubility in peraluminous melts. Terra Cognita 8, 71.

Murphy, M.A., Yin, A., Harrison, T.M., Dürr, S.B., Chen, Z., Ryerson, F.J., Kidd, W.S.F., Wang, X., Zhou, X., 1997. Did the Indo-Asian collision alone create the Tibetan Plateau? Geology 25, 719–722.

Niu, Y.L., Zhao, Z.D., Zhu, D.C., Mo, X.X., 2013. Continental collision zones are primary sites for net continental crust growth – A testable hypothesis. Earth-Science Reviews 127, 96–110.

Pan, G.T, Ding, J., Yao, D.S, Wang, L.Q., 2004. Guidebook of 1:1500000 geologic map of the Qinghai–Xizang (Tibet) plateau and adjacent areas. Chengdu, China, Chengdu Cartographic Publishing House, 1–48 (in Chinese).

Pearcy, J.G., DeBari, S.M., Sleep, N.H., 1990. Mass balance calculations for two sections of island arc crust and implications for the formation of continents. Earth and Planetary Science Letters 96, 427–442.

Petford, N., Atherton, M., 1996. Na-rich partial melts from newly underplated basaltic crust: the Cordillera Blanca Batholith, Peru. Journal of Petrology 37, 1491–1521.

Rapp, R.P., Watson, E.B., Miller, C.F., 1991. Partial melting of amphibolite/eclogite and the origin of Archean trondhjemites and tonalites. Precambrian Research 51, 1–25.

Rickwood, P.C., 1989. Boundary lines within petrologic diagrams which use oxides of major and minor elements. Lithos 22, 247–263.

Rollinson, H.R., 1993. Using Geochemical Data: Evaluation, Presentation, Interpretation. Longman Scientific & Technical, London 1–352.

Sandiford, M., Hand, M., McLaren, S., 1998. High geothermal gradient metamorphism during thermal subsidence. Earth and Planetary Science Letters 163, 149–165.

Schärer, U., Xu, R.H., Allègre, C.J., 1986. U-(Th)-Pb systematics and ages of Himalayan leucogranites, South Tibet. Earth and Planetary Science Letters 77, 35–48.

Sisson, T.W., Ratajeski, K., Hankins, W.B., Glazner, A.F., 2005. Voluminous granitic magmas from common basaltic sources. Contributions to Mineralogy and Petrology 148, 635–661.

Stern, R.J., 2002. Subduction zones. Reviews of Geophysics 40, 1012, doi:10.1029/2001RG000108.

Sui, Q.L., Wang, Q., Zhu, D.C., Zhao, Z.D., Chen, Y., Santosh, M., Hu, Z.C., Yuan, H.L., Mo, X.X., 2013. Compositional diversity of ca. 110 Ma magmatism in the northern Lhasa Terrane, Tibet: Implications for the magmatic origin and crustal growth in a continent-continent collision zone. Lithos 168-169, 144–159.

Sun, S.S., McDonough, W.F., 1989. Chemical and isotope systematics of oceanic basalts: implications for mantle composition and processes. In: Saunders, A.D. (Eds.), Magmatism in ocean Basins. Geological Society Publication 42, 313–345.

Tang, J.X., Li, F.J., Li, Z.J., Zhang, L., Tang, X.Q., Deng, Q., Lang, X.H., Huang, Y., Yao, X.F., Wang, Y., 2010. Time limit for formation of main geological bodies in Xiongcun copper–gold deposit, Xietongmen County, Tibet: evidence from zircon U–Pb ages and Re–Os age of molybdenite. Mineral Deposits 29, 461–475 (in Chinese with English abstract).

Trumbull, R.B., Wittenbrink, R., Hahne, K., Emmermann, R., Büsch, W., Gerstenberger, H., Siebel, W., 1999. Evidence for late Miocene to recent contamination of arc andesites by crustal melts in the Chilean Andes (25–26°S) and its geodynamic implications, Journal of South American Earth Sciences 12, 135–155.

van de Zedde, D.M.A., Wortel, M.R.J., 2001. Shallow slab detachment as a transient source of heat at mid lithospheric levels. Tectonics 20, 868–882.

Vervoort, J.D., Patchett, P.J., Blichert-Toft, J., Albarede, F., 1999. Relationships between Lu–Hf and Sm–Nd isotopic systems in the global sedimentary system. Earth and Planetary Science Letters 168, 79–99.

Vervoort, J.D., Patchett, P.J., Söderlund, U., Baker, M., 2004. The isotopic composition of Yb and the precise and accurate determination of Lu concentrations and Lu/Hf ratios by isotope dilution using MC-ICPMS. Geochemistry, Geophysics, Geosystems 5, Q11002, doi:10.1029/2004GC000721.

Vervoort, J.D., Plank, T., Prytulak, J., 2011. The Hf–Nd isotopic composition of marine sediments. Geochimica et Cosmochimica Acta 75, 5903–5926.

Volkmer, J.E., Kapp, P., Guynn, J.H., Lai, Q., 2007. Cretaceous-Tertiary structural evolution of the north central Lhasa Terrane, Tibet. Tectonics 26, TC6007, doi: 6010.1029/2005TC001832.

Watson, E.B., Harrison, T.M., 1983. Zircon saturation revisited: temperature and composition effects in a variety of crustal magma types. Earth and Planetary Science Letters 64, 295–304.

Wen, D.R., 2007. The Gangdese Batholith, southern Tibet: Ages, geochemical characteristics and petrogenesis. Ph.D thesis, National Taiwan University, p. 1–120.

Wen, D.R., Chung, S.L., Song, B., Iizuka, Y., Yang, H.J., Ji, J.Q., Liu, D.Y., Gallet, S., 2008b. Late Cretaceous Gangdese intrusions of adakitic geochemical characteristics, SE Tibet: petrogenesis and tectonic implications. Lithos 105, 1–11.

Wen, D.R., Liu, D.Y., Chung, S.L., Chu, M.F., Ji, J.Q., Zhang, Q., Song, B., Lee, T.Y., Yeh, M.W., Lo, C.H., 2008a. Zircon SHRIMP U–Pb ages of the Gangdese batholith and implications for Neotethyan subduction in southern Tibet. Chemical Geology 252, 191–201.

Whalen, J.B., Currie, K.L., Chappell, B.W., 1987. A-type granites: geochemical characteristics, discrimination and petrogenesis. Contributions to Mineralogy and Petrology 95, 407–419.

White, W.M., Albarède, F., Télouk, P., 2000. High-precision analysis of Pb isotope ratios using multi-collector ICP-MS. Chemical Geology 167, 257–270.

Wigger, P.J., Schmitz, M., Araneda, M., Asch, G., Baldzuhn, S., Giese, P., Heinsohn,

W.-D., Martinez, E., Ricaldi, E., Röwer, P., and Viramonte, J., 1994, Variation in the crustal structure of the southern Central Andes deduced from seismic refraction investigations, in Reutter, J., Scheuber, E., and Wigger, P. J., eds., Tectonics of the southern Central Andes: Berlin, Springer, p. 23–48.

Wu, F.Y., Jahn, B.M., Wilde, S.A., Lo, C.H., Yui, T.F., Lin, Q., Ge, W.C., Sun, D.Y., 2003. Highly fractionated I-type granites in NE China (I): geochronology and petrogenesis. Lithos 66, 241–273.

Wu, F.Y., Li, X.H., Yang, J.H., Zheng, Y.F., 2007. Discussions on the petrogenesis of granites. Acta Petrologica Sinica 23, 1217–1238 (in Chinese with English abstract).

Wu, F.Y., Yang, Y.H., Xie, L.W., Yang, J.H., Xu, P., 2006. Hf isotopic compositions of the standard zircons and baddeleyites used in U–Pb geochronology. Chemical Geology 234, 105–126.

Xia, B., Xu, L.F., Zhang, Y.Q., Deng, X.Y., Li, J.F., Wei, Z.Q., Wang, Y.B., 2008. SHRIMP zircon U-Pb dating of granodiorites from Xietongmen pluton, Tibet and its geological implication. Geotectonica et Metallogenia 32, 238–242 (in Chinese with English abstract).

Xu, W.C., 2010. Spatial variation of zircon U-Pb ages and Hf isotopic compositions of the Gangdese granitoids and its geologic implications. Unpublished result. PhD thesis, China University of Geosciences (Wuhan).

Yang, J.H., Chung, S.L., Wilde, S.A., Wu, F.Y., Chu, M.F., Lo, C.H., Fan, H.R., 2005. Petrogenesis of post-orogenic syenites in the Sulu Orogenic Belt, East China: geochronological, geochemical and Nd–Sr isotopic evidence. Chemical Geology 214, 99–125.

Yin, A., Harrison, T.M., 2000. Geologic evolution of the Himalayan-Tibetan orogen. Annual Review of Earth and Planetary Sciences 28, 211–280.

Yurimoto, H., Duke, E.F., Papike, J.J., Shearer, C.K., 1990. Are discontinuous chondrite-normalized REE patterns in pegmatitic granite systems the results of monazite fractionation? Geochimica et Cosmochimica Acta 54, 2141–2145.

Zandt, G., Velasco, A. A., and Beck, S. L., 1994, Composition and thickness of the southern Altiplano crust, Bolivia. Geology 22, 1003–1006.

Zeng, L.S., Gao, L.E., Xie, K.J., Zeng, L.J., 2011. Mid-Eocene high Sr/Y granites in the Northern Himalayan gneiss dome: melting thickened lower continental crust. Earth and Planetary Science Letters 303, 251–266.

Zhang, S.Q., Mahoney, J.J., Mo, X.X., Ghazi, A.M., Milani, L., Crawford, A.J., Guo, T.Y., Zhao, Z.D., 2005. Evidence for a widespread Tethyan upper mantle with Indian-Ocean-type isotopic characteristics. Journal of Petrology 46, 829–858.

Zhang, Z.L., Tian, L.F., Fan, Y.G., Fang, Y.Y., Jia, J.C., G, J., Wang, L.J., Lu, Y.M., Wei, W.T., Guo, J.C., Feng, G.X., Sun, X., Wu, X.G., Dong, S.J., L, G.D., Liu, L.X., Sun, L.X., Li, X., 2003. 1: 250, 000 geological report of Sangsang County with geological map. Chengdu University of Technology, Chengdu, (unpublished, in Chinese).

Zhu D.C., Wang, Q., Zhao, Z.D., Chung, S.L., Cawood, P.A., Niu, Y.L., Liu, S.A., Wu, F.Y., Mo, X.X., 2015. Magmatic record of India-Asia collision. Scientific Reports 5, 14289, doi: 10.1038/srep14289.

Zhu, D.C., Mo, X.X., Niu, Y.L., Zhao, Z.D., Wang, L.Q., Liu, Y.S., Wu, F.Y., 2009. Geochemical investigation of Early Cretaceous igneous rocks along an east–west traverse throughout the central Lhasa Terrane, Tibet. Chemical Geology 268, 298–312.

Zhu, D.C., Pan, G.T., Chun, S.L., Liao, Z.L., Wang, L.Q., Li, G.M., 2008. SHRIMP zircon age and geochemical constraints on the origin of Early Jurassic volcanic rocks from the Yeba Formation, southern Gangdese in south Tibet. International Geology Review 50, 442–471.

Zhu, D.C., Zhao, Z.D., Niu, Y., Dilek, Y., Wang, Q., Ji, W.H., Dong, G.C., Sui, Q.L., Liu, Y.S., Yuan, H.L., 2012. Cambrian bimodal volcanism in the Lhasa Terrane, southern Tibet: Record of an early Paleozoic Andean-type magmatic arc in the Australian proto-Tethyan margin. Chemical Geology 328, 290–308.

Zhu, D.C., Zhao, Z.D., Niu, Y.L., Dilek, Y., Hou, Z.Q., Mo, X.X., 2013. The origin and pre-Cenozoic evolution of the Tibetan Plateau. Gondwana Research 23, 1429–1454.

Zhu, D.C., Zhao, Z.D., Niu, Y.L., Mo, X.X., Chung, S.L., Hou, Z.Q., Wang, L.Q., Wu, F.Y., 2011. The Lhasa Terrane: Record of a microcontinent and its histories of drift and growth. Earth and Planetary Science Letters 301, 241–255.

Figure captions

Fig.1. (a) Tectonic framework of the Tibetan Plateau (Zhu et al., 2013) showing major tectonic subdivisions; (b) Simplified geological map of Lhasa Terrane showing the main tectonic units (Zhu et al., 2011) and spatial and temporal distribution of ca. 43 ± 3 Ma magmatic rocks (ovals with numerals); (c) Geological map of Dajia area (Zhang et al., 2003). Abbreviations: JSSZ = Jinsha Suture Zone, BNSZ = Bangong-Nujiang Suture Zone, SNMZ = Shiquan River-Nam Tso Mélange Zone, LMF = Luobadui-Milashan Fault, IYZSZ = Indus-Yarlung Zangbo Suture Zone, SL = southern Lhasa subterrane, CL = central Lhasa subterrane, NL = northern Lhasa subterrane. Literature data are from Harrison et al. (2000), Wen et al. (2008a), Dong (2008), Xia et al. (2008), Ji et al. (2009, 2012), Xu (2010), Ji (2010), Tang et al. (2010), Huang et al. (2010), Dong et al. (2011), Guan et al. (2012), Cong et al. (2012), Jia (2014), and our unpublished data.

Fig.2. Photomicrographs showing the texture of the Dajia pluton in the western Gangdese Batholith. Abbreviations: Pl = plagioclase, Kfs = K-feldspar, Q = quartz.

Fig.3. Cathodoluminescence (CL) images of representative zircons and concordia diagrams of three samples of Dajia pluton in the western Gangdese Batholith. Solid and dashed circles indicate the locations of LA-ICP-MS U-Pb dating and Hf analyses, respectively. The scale bar length in CL image is 50 μm.

Fig. 4. (a) R2 vs. R1 diagram (De la Roche et al., 1980) for classification; (b) K_2O vs. SiO_2 plot (Rickwood, 1989) and (c) A/CNK vs. Differentiation Index (DI) plots showing sample compositional variation. A/CNK=Al_2O_3/(CaO+Na_2O+K_2O) (molar ratio), DI = Quartz (Qtz) + Orthoclase (Or) + Albite (Ab) + Nepheline (Ne) + Leucite (Lc) + K-feldspar (Kfs), from CIPW calculating values.

Fig.5. Selected plots of the Dajia pluton in the western Gangdese Batholith. (d) P_2O_5 vs. SiO_2 showing evolution trends of I-type and S-type magmas. Eu/Eu* = 2 × $Eu_N/(Sm_N + Gd_N)$, where N denotes normalized to chondrite values of Sun and McDonough (1989).

Fig.6. Chondrite-normalized REE and primitive-mantle-normalized trace element

patterns of the Dajia pluton. Normalization data are from Sun and McDonough (1989).

Fig.7. (a) Whole-rock $\varepsilon_{Nd}(t)$ vs. $\varepsilon_{Hf}(t)$ of of the Dajia pluton. The compositions of end-members used for mixing calculations are: the Gangdese mafic lower crust (represented by a gabbro sample of ST141A; Wen et al., 2008b): $\varepsilon_{Nd}(t)$ = 3.5, Nd = 20.0 ppm, Hf = 2.78 ppm (Wen, 2007), $\varepsilon_{Hf}(t)$ = 11.1 (Chu et al., 2011); the Lhasa basement-derived melt (represented by a strongly peraluminous granite sample of 08DX17; Zhu et al., 2011): $\varepsilon_{Nd}(t)$ = −16.2, Nd = 43.40 ppm, Hf = 4.32 ppm, averaged zircon $\varepsilon_{Hf}(t)$ = −21.8; the Himalayan sediments: $\varepsilon_{Nd}(t)$ = −13.4, $\varepsilon_{Hf}(t)$ = −20.0, Nd = 27 ppm, Hf = 4.06 ppm (Chauvel et al., 2008). The terrestrial array is from Vervoort et al. (1999); (b) $(^{207}Pb/^{204}Pb)i$ vs. $(^{206}Pb/^{204}Pb)i$ and (c) $(^{208}Pb/^{204}Pb)i$ vs. $(^{206}Pb/^{204}Pb)i$ of the Dajia pluton. Data sources: Leucogranites and gneiss in the central Lhasa subterrane (Gariépy et al., 1985; Liao, 2003), Himalayan basement (Gariépy et al., 1985; Schärer et al., 1986), Yarlung Zangbo Ophiolite (Zhang et al., 2005), and Tethyan subduction-related rocks in the southern Lhasa subterrane (Gariépy et al., 1985; Zhu et al., 2008). Northern Hemisphere Reference Line (NHRL): $(^{207}Pb/^{204}Pb)_{NHRL} = 0.1084 \times (^{206}Pb/^{204}Pb)i + 13.491$, $(^{208}Pb/^{204}Pb)_{NHRL} = 1.209 \times (^{206}Pb/^{204}Pb)i + 15.627$ (Hart, 1984). All initial isotopic ratios are corrected to t = 43 Ma.

Fig.8. (a) Plots of $\varepsilon_{Hf}(t)$ vs. ages of the ca. 43 Ma magmatism in the Gangdese Batholith. The sub-horizontal lines are Hf "crustal" model ages (T_{DM}^{C}), which are calculated by assuming its parental magma to have been derived from an average continental crust (with $^{176}Lu/^{177}Hf$=0.015) that originated from the depleted mantle source (Griffin et al., 2002). Literature data are from Wen et al. (2008a), Dong (2008), Ji et al. (2009, 2012), Ji (2010), Xu (2010), Huang et al. (2010), Xu (2010), Zhu et al. (2011), Guan et al. (2012), Cong et al. (2012), Jia (2014), and our unpublished data; (b-c) Histograms of zircons $\varepsilon_{Hf}(t)$ values for Group 1 samples the and Group 2 samples.

Fig.9. Histogram of SiO_2 (wt.%) of ca. 43 ± 3 Ma magmatic rocks from the Gangdese Batholith showing that the magmatism is dominated by felsic compositions. Data sources are same as in Fig. 1.

Fig.10. (a) ($Na_2O + K_2O$)/CaO vs. Zr + Nb + Ce + Y and (b) TFeO*/MgO vs. Zr + Nb + Ce + Y plots (Whalen et al., 1987) showing that Group 2 are most likely strongly fractionated granites. Data sources are same as in Fig. 1.

Fig.11. (a) Ba vs. Sr and (b) Rb/Sr vs. Sr plots showing fractionation of plagioclase and biotite which controlled the variation of these elements from Group 1 to Group 2 samples; (c) $(La/Yb)_N$ vs. La showing the change of REE patterns from Group 1 to Group 2 samples by separation of titanite, allanite, and apatite. Partition coefficients are from Rollinson (1993), Green and Pearson (1986), Mahood and Hildreth (1983), and Yurimoto et al. (1990). Abbreviations: Pl = plagioclase, Kfs = K-feldspar, Bi = biotite, Zr = zircon, Tit = titanite, Ap = apatite, Allan = allanite, Mon = monazite.

Fig. 12. Modeled REE patterns with quantitative fractionated phase combinations. The assumed parent magma composition is represented by the least fractionated sample (12DJC13-1) of the Group 1. Partition coefficients are from Rollinson (1993) and Green and Pearson (1986). Abbreviations: Tit = titanite, Ap = apatite, Allan = allanite.

Fig. 13. Schematic illustrations showing the geodynamic evolution of India-Asia collision zone at ca. 53 Ma and ca. 43 ± 3 Ma. Abbreviations: ALC= ancient lower crust, JLC= juvenile lower crust, and SCLM = sub-continental lithospheric mantle. Modified from Zhu et al. (2015).

Wang et al. Fig. 1 W160 mm - H128 mm

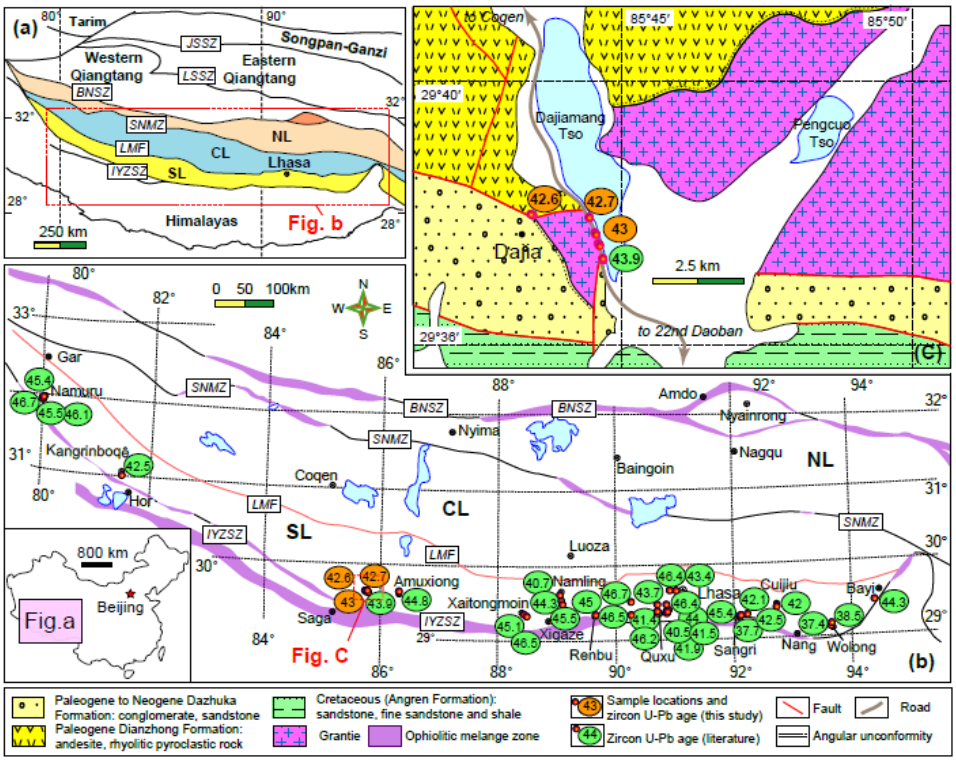

Wang et al. Fig. 2 W162 mm - H60 mm

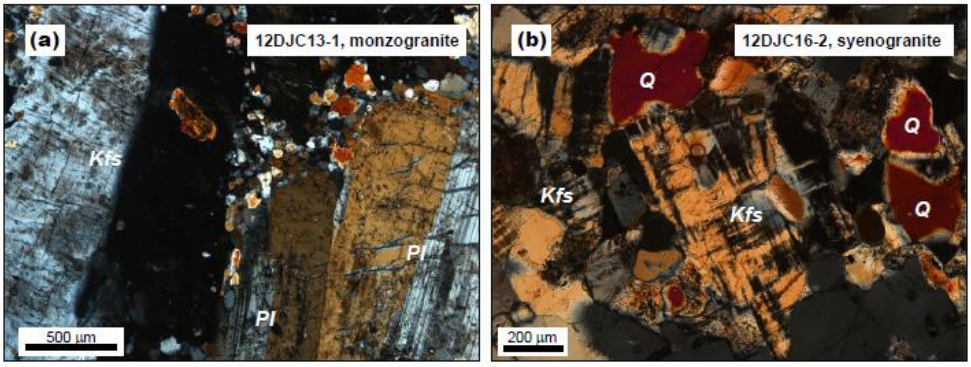

Wang et al. Fig. 3 W88 mm - H177 mm

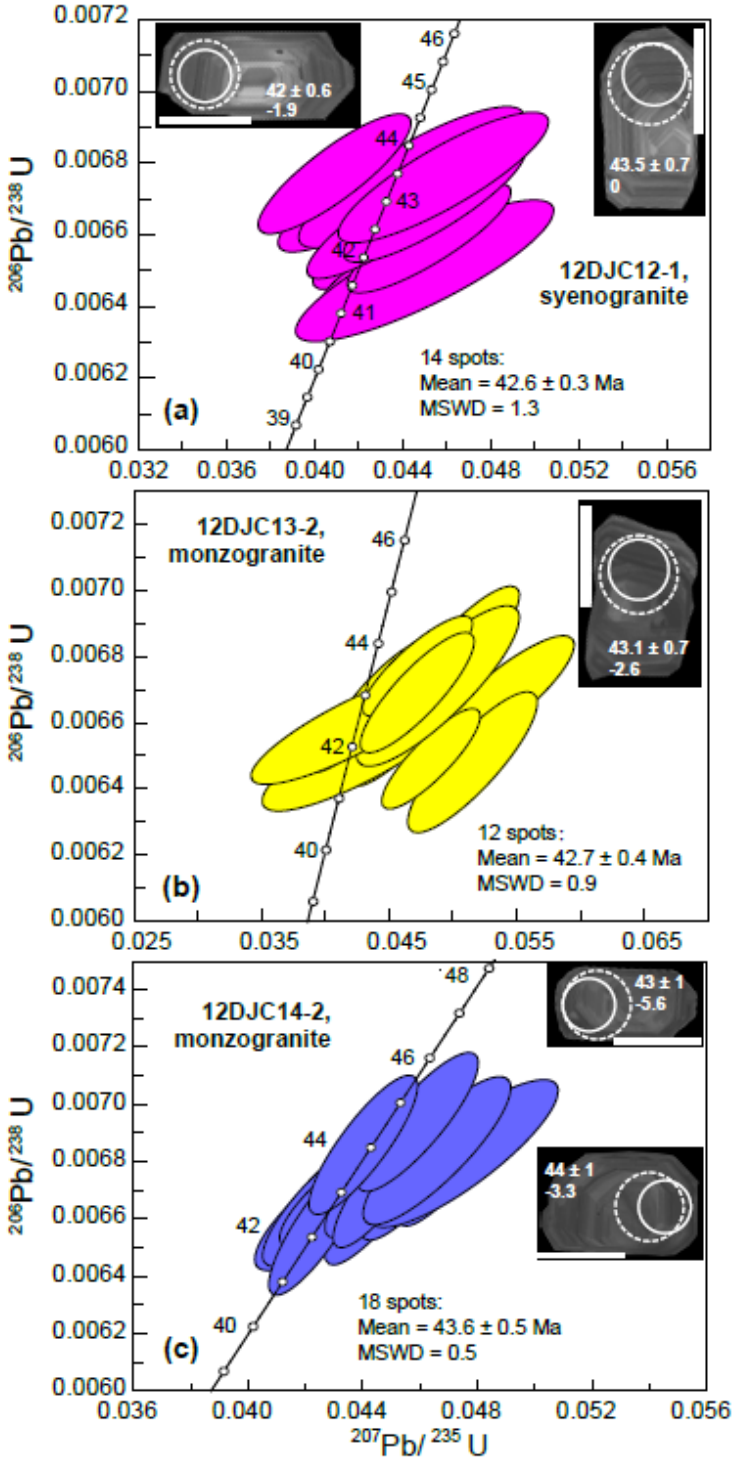

Wang et al. Fig. 4 W165 mm - H120 mm

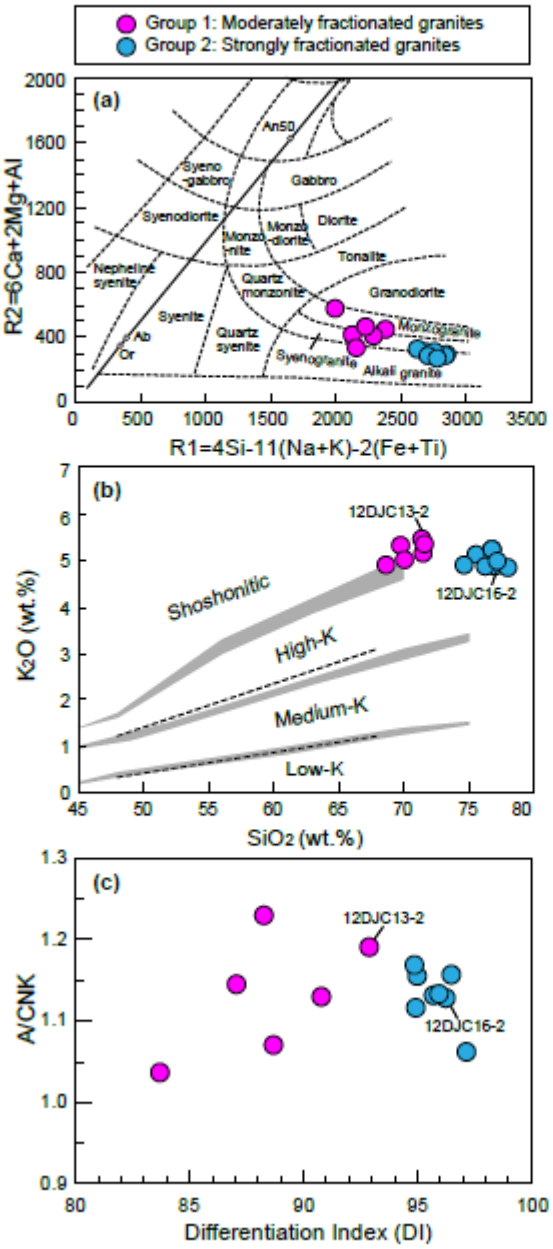

Wang et al. Fig. 5 W166 mm - H83 mm

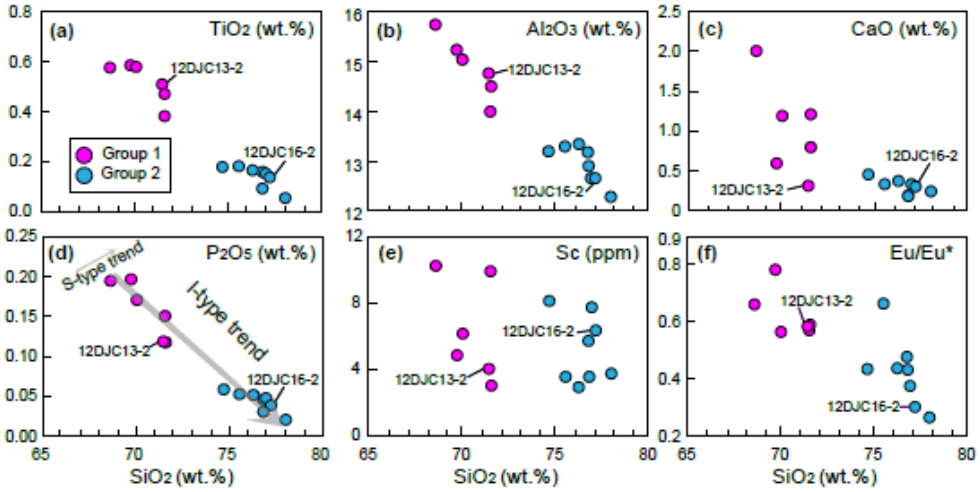

Wang et al. Fig. 6 W165 mm - H56 mm

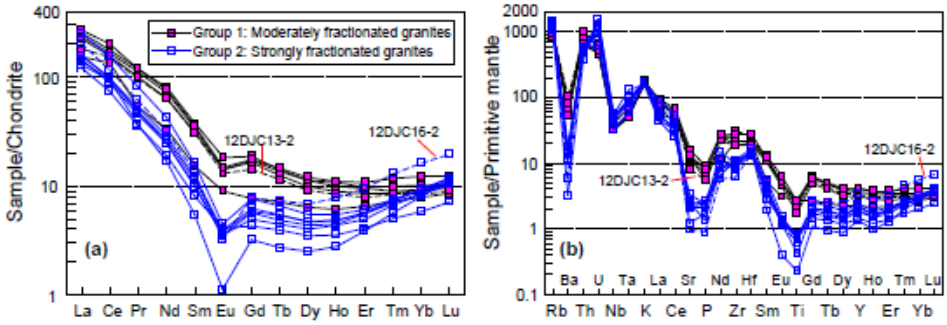

Wang et al. Fig. 7 W84 mm - H173 mm

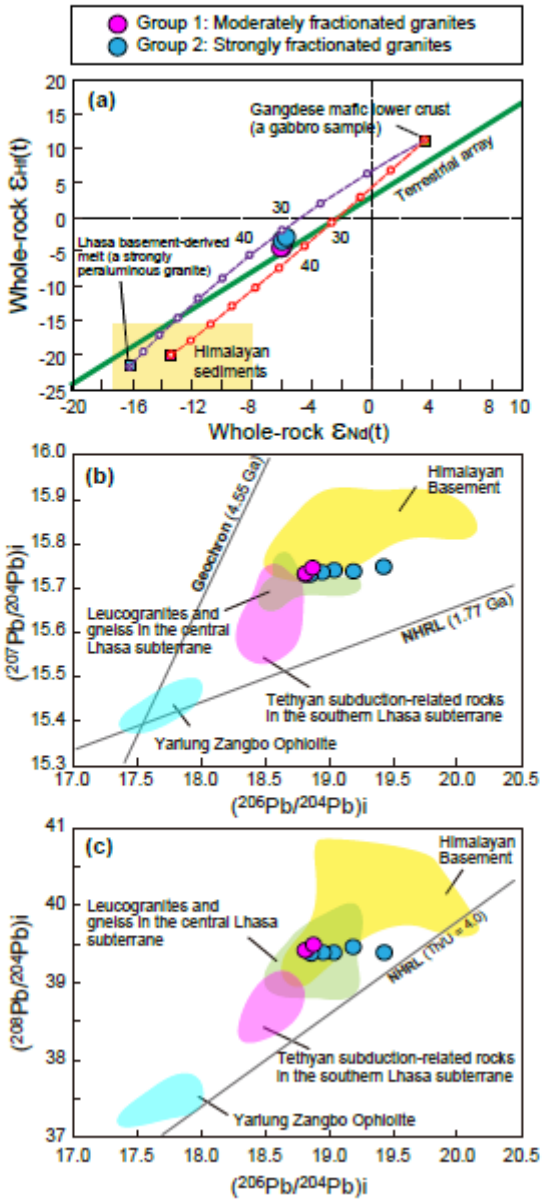

Wang et al. Fig. 8 W161 mm - H87 mm

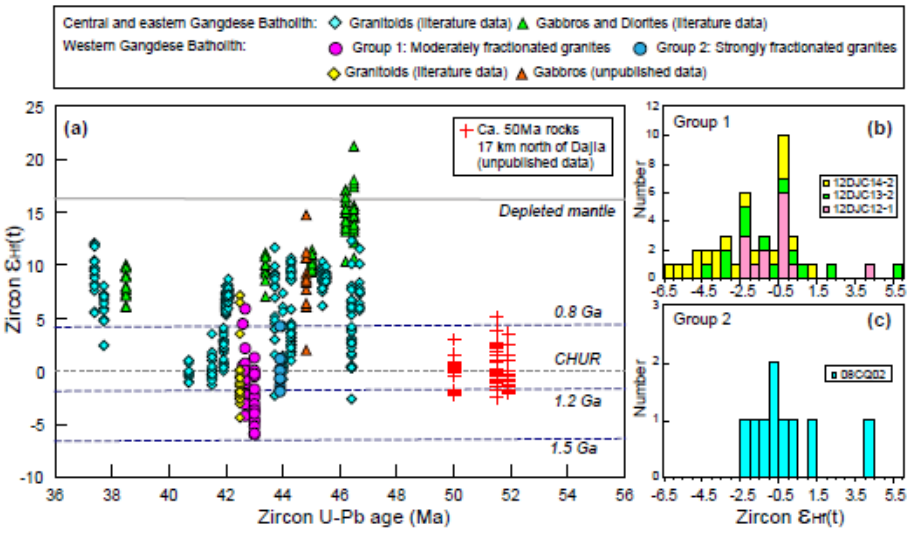

Wang et al. Fig. 9 W81 mm - H60 mm

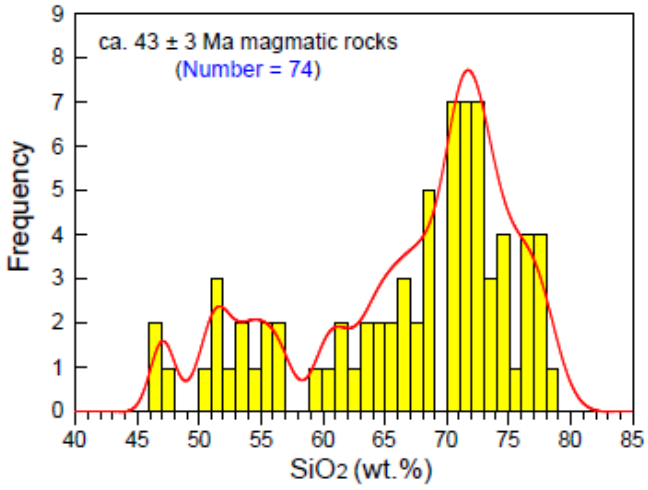

Wang et al. Fig. 10 W162 mm - H65 mm

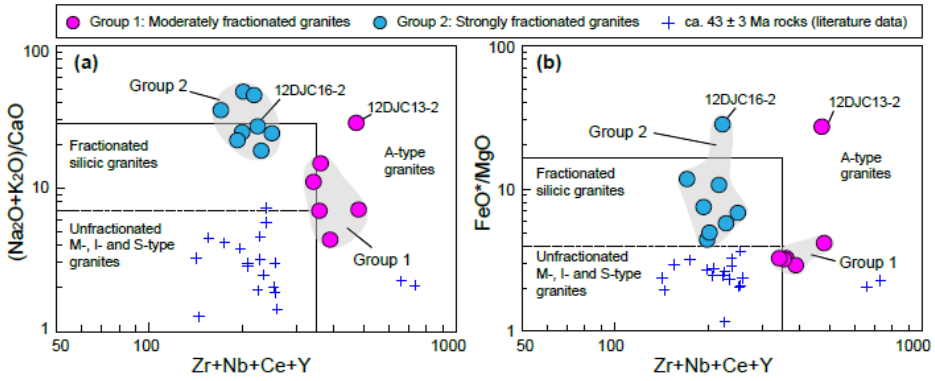

Wang et al. Fig. 11 W83 mm - H177 mm

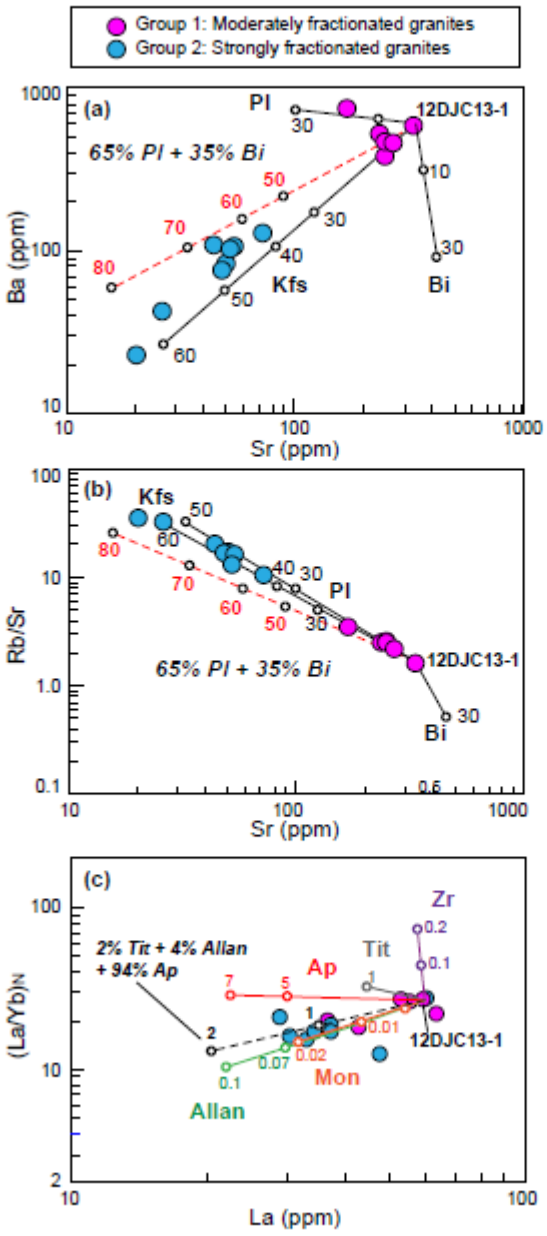

Wang et al. Fig. 12 W80 mm - H56 mm

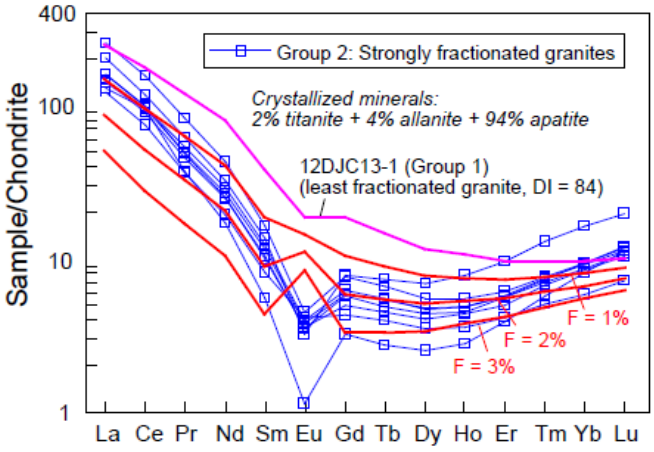

Wang et al. Fig. 13 W111 mm - H83 mm

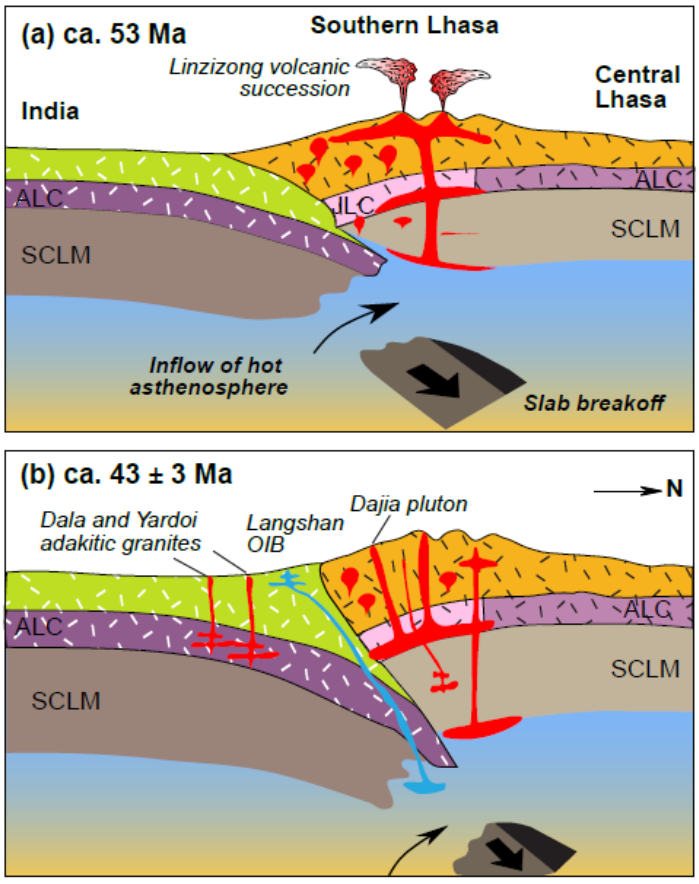

Wang and Zhu et al.'s Research Highlights

► Moderately and strongly fractionated granites were synchronously emplaced at ca. 43 Ma

► These rocks were characterized by low Y and HREEs abundances with similar Nd-Hf-Pb isotopic compositions

► Partial melting of a common garnet-bearing amphibolite accompanied with varying degrees of fractionation controlled their generation

► These rocks witnessed crustal thickening of the southern Lhasa Terrane by ca. 43 Ma.